Stochastic Analysis of Turbulence

Robert Stresing

Von der Fakultät für Mathematik und Naturwissenschaften
der Carl von Ossietzky Universität Oldenburg
zur Erlangung des Grades und Titels eines

DOKTORS DER NATURWISSENSCHAFTEN
DR. RER. NAT.

angenommene Dissertation

von Herrn Robert Stresing
geboren am 31.01.1979 in Wilhelmshaven

Gutachter: Prof. Dr. Joachim Peinke
Zweitgutachter: Prof. Dr. Rudolf Friedrich
Tag der Abgabe: 13.05.2010
Tag der Disputation: 11.08.2010

Für Carmen.

Contents

Abstract

The subject matter of the present work is the stochastic analysis of turbulence based on the theory of Markov processes.

We apply this method in Chapter 2 to turbulence generated by a fractal square grid. We examine the stochastic cascade process of nested velocity increments in scale, which is governed by a Fokker-Planck equation. From this analysis, the joint multi-scale statistics of velocity increments can be obtained. In stark contrast to all documented boundary-free turbulent flows, we find that these multi-scale statistics, the coefficients of the Fokker-Planck equation, and dissipation-range intermittency are all practically independent of the Reynolds number (the characteristic ratio of inertial to viscous forces in the fluid). These properties define a qualitatively new class of turbulence.

In Chapter 3, we study the Markov properties of experimental velocity data from different homogeneous isotropic turbulent flows. We find that consistent estimates of the so-called Einstein-Markov coherence length, which is closely related to the Taylor microscale, can be obtained for different nesting structures of velocity increments. We also analyze the stochastic process of the velocity in time, or, by Taylor's hypothesis, equivalently in space. Although this process does not have the exact Markov property, we can identify the same Einstein-Markov coherence length as for the stochastic processes in scale. Using a method based on the matrix of transition probabilities, we examine the limits of Markov chain models for the turbulent velocity.

Furthermore, we show in Chapter 4 how the stochastic analysis of the interscale process can be extended in order to obtain the complete multi-point statistics of the velocity field. We condition the stochastic cascade process on the velocity value itself, and find that the resulting process is also governed by a Fokker-Planck equation, which contains a simple additional velocity-dependent term in the drift function. Taking into account this additional term, the multi-point statistics can be expressed by three-point statistics of the velocity field. Thus, we propose a stochastic three-point closure for the velocity field of homogeneous isotropic turbulence.

In Chapter 5, we present further results on inhomogeneous turbulence, fractal-generated turbulence, the Markov property, and multi-point statistics.

Zusammenfassung

Gegenstand der vorliegenden Arbeit ist die stochastische Analyse der Turbulenz auf der Grundlage der Theorie der Markovprozesse.

Wir verwenden diese Methode in Kapitel 2 zur Untersuchung einer turbulenten Strömung, die durch ein fraktales Gitter mit quadratischer Grundstruktur erzeugt wurde. Wir untersuchen den stochastischen Kaskadenprozess von ineinander geschachtelten Geschwindigkeitsinkrementen, der von einer Fokker-Planck-Gleichung bestimmt wird. Aus dieser Analyse kann die Mehrskalen-Verbundwahrscheinlichkeit der Geschwindigkeitsinkremente gewonnen werden. Im Gegensatz zu allen anderen bisher untersuchten freien turbulenten Strömungen sind die Koeffizienten der Fokker-Planck-Gleichung und die Mehrskalen-Statistik, sowie die Intermittenz im Dissipationsbereich nahezu unabhängig von der Reynoldszahl (dem charakteristischen Verhältnis von Trägheits- und Zähigkeitskräften im Fluid). Durch diese Eigenschaften wird eine qualitativ neue Klasse der Turbulenz definiert.

In Kapitel 3 untersuchen wir die Markoveigenschaften experimenteller Geschwindigkeitsdaten von verschiedenen homogenen und isotropen turbulenten Strömungen. Wir zeigen, dass die sogenannte Einstein-Markov-Kohärenzlänge, welche eng mit der Taylorlänge in Beziehung steht, für verschiedene Arten der Schachtelung der Geschwindigkeitsinkremente auf konsistente Weise ermittelt werden kann. Außerdem untersuchen wir den stochastischen Prozess der Geschwindigkeit in der Zeit, beziehungsweise, nach der Taylorhypothese, im Raum. Obwohl dieser Prozess keine exakte Markoveigenschaft aufweist, kann dieselbe Einstein-Markov-Kohärenzlänge wie für den Skalenprozess bestimmt werden. Wir verwenden eine Methode auf der Grundlage von Übergangswahrscheinlichkeits-Matrizen, um die Grenzen von Markov-Ketten-Modellen für die turbulente Geschwindigkeit zu untersuchen.

Darüber hinaus zeigen wir in Kapitel 4, wie die stochastische Analyse des Skalenprozesses erweitert werden kann, um die vollständige Mehrpunktstatistik des Geschwindigkeitsfeldes zu erhalten. Wir bedingen den stochastischen Kaskadenprozess auf die Geschwindigkeit selbst und stellen fest, dass der daraus resultierende Prozess ebenfalls durch eine Fokker-Planck-Gleichung beschrieben wird, die einen

zusätzlichen, geschwindigkeitsabhängigen Term in der Driftfunktion enthält. Unter Berücksichtigung dieses einfachen zusätzlichen Terms kann die Mehrpunktstatistik durch Drei-Punkt-Statistiken des Geschwindigkeitsfeldes ausgedrückt werden. Somit schlagen wir eine stochastische Dreipunkt-Schließung des Geschwindigkeitsfeldes homogener, isotroper Turbulenz vor.

In Kapitel 5 stellen wir weitere Ergebnisse zu inhomogener Turbulenz und mittels fraktaler Gitter erzeugter Turbulenz, sowie zur Markoveigenschaft und zur Mehrpunktstatistik vor.

Chapter 1

Introduction

Complex systems are characterized by the existence of structures at different scales. The multitude or even infinity of appearances which those structures might assume calls for a statistical description of complex systems in general, and of turbulent flows, which are the subject matter of the present work, in particular. The observation that such structures might be similar, but not necessarily identical, at different scales, calls for a scale-dependent statistical description. Since an exact solution of the equations of motion by means of numerical simulation is still far beyond the possibilities of the available computing power for most turbulent flows — and will remain so for a long time —, any substantial progress in the statistical description and theory of turbulence will possess a great value for many fields of research, from various areas of engineering to weather, climate and ocean dynamics, geo- and astrophysics and even cosmology.

A scale-dependent statistical description of turbulence is given by the probability density function (PDF) $p[\xi(r)]$ of a quantity ξ at different scales r.[1] The most commonly used scale-dependent quantity is the (longitudinal) velocity increment

$$\begin{aligned} \xi(r) &= U(x+r) - U(x) \\ &= u(x+r) - u(x) \end{aligned} \tag{1.1}$$

[1] Throughout this book, different types of brackets, $(\cdot)$ and $[\cdot]$, are used to facilitate reading. The notation $p[\xi(r)]$ is equivalent to $p[\xi, r]$.

where $U(x)$ is the velocity at the point x, and $u(x)$ is the *fluctuating* velocity, $u(x) \equiv U(x) - \bar{U}$, with the mean flow velocity $\bar{U}$. The characterization of turbulence by means of the PDF $p[\xi(r)]$, or, equivalently, by its moments of order n, $S_n(r) \equiv \langle \xi(r)^n \rangle$, the so-called structure functions, has been the principal focus of turbulence research since the pioneering works of Kolmogorov [1, 2, 3].

Since the large scales of a turbulent flow, that is, scales of the order of the flow width or the size of the turbulence-generating object, are naturally dominated by the specific boundary conditions, the hopes for unification and the emergence of a "proper theory of turbulence" rely on the small scales [4]. The hypothesis of *universality* of small-scale turbulence is central to all statistical theories of turbulence and to all turbulence models used for numerical simulation. Specifically, it is assumed that turbulent flows have universal statistical properties at small scales in the limit of infinite Reynolds number *Re*. The Reynolds number is defined as

$$Re = \frac{U_0 L_0}{\nu}, \tag{1.2}$$

where U_0 is a typical velocity (e.g. the mean value $\bar{U}$ or the standard deviation u_{rms} of the flow velocity), L_0 is a typical length scale of the flow, and ν is the kinematic viscosity of the fluid. The length scale L_0 might be defined as the flow width or the diameter of the turbulence-generating object, or as an intrinsic scale of the flow like the *integral length scale*, which is defined as the integral $L = \int_0^\infty f(r)\mathrm{d}r$ over the autocorrelation function $f(r) = \langle u(x+r)u(x) \rangle / \langle u(x)^2 \rangle$. The Reynolds number is a measure of the ratio of inertial to viscous forces in a flow.

The idea of universality of small-scale turbulence is closely related to the concept of the *energy cascade*, which dates back to Richardson [5]. In this picture, energy is inserted into the flow at large scales and transported to very small scales in a process where structures like eddies repeatedly split up, transferring their kinetic energy to smaller and smaller structures, where it finally dissipates into heat. The range of scales which are small compared to the large, energy containing structures, but large compared to the scales where dissipation plays a role, is called the inertial range. The inertial range extends down to *at least* the so-called Taylor microscale λ [6], and dissipation finally dominates at scales of the order of magnitude of the Kolmogorov scale, or dissipation

scale, η. In his famous "Statistical Theory of Turbulence" [7], Taylor shows for the energy dissipation rate per unit mass, ε, for isotropic turbulence that

$$\varepsilon = 15\nu\frac{u_{rms}^2}{\lambda^2}, \tag{1.3}$$

where $u_{rms} = \sqrt{\langle u^2 \rangle}$ is the standard deviation of the fluctuating velocity.[2] In the same work, Taylor presents experimental evidence for the assumption that

$$\varepsilon = C_\varepsilon \frac{u_{rms}^3}{L}, \tag{1.4}$$

where L is the integral scale and C_ε is a dimensionless constant which is independent of the Reynolds number in the limit of $Re \to \infty$. This equation is the expression of the "dissipation anomaly", which states that the dissipation does not depend on the viscosity ν, and therefore not on the Reynolds number, in the limit of $Re \to \infty$. The dissipation anomaly is related to the experimental observation that the drag coefficient of an object in a flow is independent of the Reynolds number for high Reynolds numbers [6]. Various experiments and numerical simulations seem to confirm that C_ε is independent of Reynolds number in the limit of high Reynolds numbers [8, 9, 10, 11, 12]. The assumption that ε is independent of the viscosity ν is central for most theories of turbulence including Kolmogorov's work [1, 2, 3, 13], and for turbulence models used for numerical simulation. Combining equations (1.3) and (1.4), and defining the Reynolds number as $Re = u_{rms}L/\nu$, we obtain the proportionality $\sqrt{Re} \propto L/\lambda$.[3] Therefore, in the Richardson-Kolmogorov phenomenology, the inertial range must become larger with increasing Reynolds number.

The generation of a type of fully developed turbulence which is homogeneous and isotropic but does *not* obey the Richardson-Kolmogorov phenomenology is of great interest for turbulence research. Such a type of turbulence has been found recently by Vassilicos and

[2] Also denoted $u_{rms} \equiv \sigma_u$.

[3] The Taylor microscale-based Reynolds number, R_λ, is defined as $R_\lambda = u_{rms}\lambda/\nu$. It is proportional to the square root of the Reynolds number based on large scales like the integral scale: $R_\lambda \propto \sqrt{Re}$. The Richardson-Kolmogorov phenomenology thus leads to the proportionality $R_\lambda \propto L/\lambda$.

coworkers [14, 15, 16]. It is generated in a wind tunnel with a grid with *fractal* structure, which perturbs the flow at several scales simultaneously. This fractal-generated turbulence has very different properties compared to all other types of turbulence previously studied. The most significant difference to "regular" (i.e. not fractal-generated) turbulence is that the ratio of the integral length over the Taylor microscale is independent of the Reynolds number. Thus, fractal-generated turbulence scales with a single length scale instead of two distinct outer (integral) and inner (Taylor or Kolmogorov) scales. Consequently, the parameter C_ε in Eq. (1.4) can not be independent of the Reynolds number, and there is no dissipation anomaly in fractal-generated turbulence.

Furthermore, it has been observed for fractal-generated turbulence that, as the Reynolds number increases, the level of small-scale intermittency remains constant and the average vortex stretching diminishes [17]. Small-scale intermittency (or more precisely, dissipation-range intermittency [6]) can be quantified by the derivative flatness, $F \equiv \langle (\frac{\partial u}{\partial x})^4 \rangle / \langle (\frac{\partial u}{\partial x})^2 \rangle^2$, which increases with Reynolds number for regular turbulence [18, 17]. Vortex stretching can be quantified by the derivative skewness, $S \equiv \langle (\frac{\partial u}{\partial x})^3 \rangle / \langle (\frac{\partial u}{\partial x})^2 \rangle^{3/2}$, which is a normalized measure of the average rate of enstrophy generation by vortex stretching in homogeneous isotropic turbulence (enstrophy is the average of half the square of the vorticity $\nabla \times \vec{u}$) [17]. The phenomenon of increasing vortex stretching is directly related to one of the "Millennium Problems" of mathematics, the one concerned with the regularity of the solutions of the Navier-Stokes equations which govern fluid flow [19].

At this point we should mention that all we have said about regular and fractal-generated turbulence applies to freely decaying turbulence, that is, turbulence where the external forcing, the mechanism through which energy is inserted into the flow, is not present any more. In the case of turbulence generated by regular or fractal grids, the state of freely decaying turbulence is established at a sufficiently large distance downstream of the grid [14, 15].

The energy of regular turbulence decays following a power law, $u_{rms}^2 \propto t^{-\kappa}$, where t is the time, and the exponent κ has been found to be larger than one [20]. A power-law decay is only one possible similarity solution of the spectral equations for the decay of isotropic turbulence [21, 22]. Another possible solution is *exponentially* decaying turbulence, which scales with a single constant length scale [22, 23]. In fact, fractal-generated turbulence decays exponentially with

$u_{rms}^2 \propto \exp[-(x - x_{\text{peak}})/\lambda]$, where the distance from the grid x is proportional to time t, and x_{peak} is the distance where u_{rms} has its maximum [15]. As predicted by George and Wang [22], the exponential decay of fractal-generated turbulence comes along with a constant ratio of L/λ.

Finally, we should mention that fractal-generated turbulence is not only interesting from the point of view of turbulence theory. On the contrary, most natural objects which generate turbulence in the atmosphere, like mountains and trees, have approximately fractal structure, or do at least generate turbulence at more than one scale.

In the description of turbulence by means of increment-PDFs $p[\xi(r)]$, information about the interaction between different scales is missing, in the sense that the statistics are only known at each scale r independently from all other scales. A more complete characterization is given by the joint multi-scale PDF $p[\xi(r_1), \xi(r_2), \ldots, \xi(r_N)]$ of the velocity increments at N scales. Here, we consider the velocity increments always for the same point x, so that an increment at scale r_n does always lie inside the increment at the next larger scale r_{n+1}. The analysis of multi-scale statistics is greatly simplified if the stochastic process from large to small scales (or vice-versa) has Markov properties, that is if

$$p[\xi(r_n)|\xi(r_{n+1}), \xi(r_{n+2}), \ldots, \xi(r_N)] = p[\xi(r_n)|\xi(r_{n+1})], \qquad (1.5)$$

where the scales are sorted as $r_1 < r_2 < \cdots < r_N$. Note that the description of the statistics of the velocity increment as a stochastic process from large to small scales is conceptually similar to the idea of the energy cascade, although the possibility of such a description *per se* clearly does not imply the existence of the energy cascade. If equation (1.5) holds, the N-scale PDF factorizes into a product of simple conditional PDFs,

$$p[\xi(r_1), \xi(r_2), \ldots, \xi(r_N)] = \qquad (1.6)$$
$$p[\xi(r_1)|\xi(r_2)] \cdot p[\xi(r_2)|\xi(r_3)] \cdots p[\xi(r_{N-1})|\xi(r_N)] \cdot p[\xi(r_N)].$$

The evolution of these conditional PDFs in scale r can be described by a Kramers-Moyal expansion which might simplify to a Fokker-Planck

equation,

$$-r\frac{\partial}{\partial r}p[\xi(r)|\xi'(r')] = -\frac{\partial}{\partial \xi}\left[D^{(1)}(\xi,r)p[\xi(r)|\xi'(r')]\right] + \frac{\partial^2}{\partial \xi^2}\left[D^{(2)}(\xi,r)p[\xi(r)|\xi'(r')]\right], \tag{1.7}$$

where $r' > r$.[4] For a more detailed description of this formalism, see Chapter 3. For now, it is sufficient to note that the coefficients of the Fokker-Planck equation, the drift and diffusion functions $D^{(1)}(\xi,r)$ and $D^{(2)}(\xi,r)$, respectively, can be estimated directly from the measured data, in our case, from a time series of the turbulent velocity signal. It has been demonstrated for various different homogeneous isotropic turbulent flows that the stochastic cascade process of the velocity increment in fact has the Markov property, and that it can be described by a Fokker-Planck equation [25, 26, 27, 28, 29, 30, 31, 32]. This method has also been successfully applied to other complex systems like roughness of surfaces [33, 34], eathquakes [35], and financial data [36, 37, 38].

The description of the interscale process of turbulence and other complex systems is valid only for scale distances $\Delta r \equiv r_{n+1} - r_n$ which are larger than the so-called *Einstein-Markov coherence length* l_{EM}. In the case of homogeneous isotropic turbulence, this length scale is of the order of magnitude of the Taylor microscale, $l_{EM} \approx 0.8\lambda$ [39]. Therefore, the scales l_{EM} and λ are most likely related to the size of the largest coherent structures associated with viscosity, because such structures would 'smooth out' the stochastic character of the velocity field and inhibit the Markov property (see Chapter 3 and [39]).

The multi-scale description of velocity increments by a Fokker-Planck equation allows a deeper insight into the statistical properties of turbulence. Renner *et al.* [29] find that the diffusion function $D^{(2)}$ does not converge even for Reynolds numbers as high as $Re \approx 10^6$ ($R_\lambda \approx 1200$) for data from a cryogenic helium free-jet experiment. This observation questions the hypothesis of statistical independence of the Reynolds number in the limit of $Re \to \infty$, which is the presupposition of the hypothesis of universality of homogeneous isotropic small-scale turbulence.

[4] According to Pawula's theorem, the Kramers-Moyal expansion, which has an infinite number of coefficients $D^{(k)}$, truncates after the second-order coefficient, and becomes a Fokker-Planck equation, if the fourth-order coefficient $D^{(4)}$ is zero [24].

As explained above, fractal-generated turbulence differs from all other types of turbulence previously studied by the fact that it scales with a single length scale which is independent of the Reynolds number, and by the independence of dissipation-range intermittency of the Reynolds number [14, 15, 17]. In Chapter 2, we present a stochastic multi-scale analysis of fractal-generated turbulence, and find that in contrast to the results for free-jet turbulence in [29], the coefficients of the Fokker-Planck equation, and the multi-scale statistics of fractal-generated turbulence are in fact practically independent of the Reynolds number. This result confirms the special character of fractal-generated turbulence and shows that not only the intrinsic length-scales of this type of turbulence are independent of the Reynolds number, but also the deeper statistical properties which can be examined by the stochastic analysis of the cascade process. Together with the characteristics described above, these findings suggest that fractal-generated turbulence is in fact a new, previously unknown class of turbulence.

The method of stochastic analysis based on Markov properties raises some questions which we address in Chapters 3 and 4 as well as Sections 5.3 and 5.4 of the present book. One of these questions is how the stochastic process, and in particular its Markov property and the Einstein-Markov coherence length, depend on the nesting structure of the velocity increments. The definition of velocity increments given in Equation (1.1) implies a "left-bounded" nesting structure, where increments at different scales have the left point x in common. This is not the only possible nesting structure. Increments might also be centered, right-bounded, or nested in other ways. It has already been shown that the nesting structure influences the Markov property, and that left- or right-bounded increments introduce spurious correlations, that is, correlations between increments at different scales, even if the "velocity" is uncorrelated white noise [40, 41]. However, a systematic investigation of the effects of the nesting structure on the Markov property of experimental turbulence data was still missing, and will be given in Chapter 3.

In the same chapter, we also examine the Markov property of the process of the velocity u in space x or, by the so-called Taylor hypothesis, equivalently in time t. We investigate the limits of Markov models for the velocity in detail. Such models are interesting for the synthetic

generation of turbulence data (see [42, 43]), a problem which is of great importance, for example, for the investigation of the behavior of wind energy converters which operate in the turbulent atmospheric boundary layer.

Furthermore, a stochastic description of the turbulent velocity as a function of the spatial position x might open up new possibilities of turbulence modeling. For all methods of computational simulation of turbulence, except the most time-consuming —and therefore most expensive—, namely direct numerical simulation (DNS), the small-scale structure of turbulence is modeled in some way in order to avoid an explicit calculation of the small-scale dynamics. The framework of Markov processes might open the way towards a stochastic modeling of these small-scale structures, an approach which would amount to a *stochastic closure* of turbulence. The *closure problem* of fluid dynamics can be stated as follows: From the equations of motion of fluid flow, the Navier-Stokes equations, one can derive an infinite system of differential equations for all possible moments of the multi-point PDFs of the velocity field. Unfortunately, any finite subsystem of this system is always unclosed, as, for example, are the so-called Reynolds averaged Navier-Stokes (RANS) equations [44]. If the multi-point statistics at small scales could be obtained from a stochastic process with empirically accessible coefficients (drift- and diffusion functions), this process might be used to model the correlations of the components of the fluctuating velocity in the RANS equations, as we will explain in Section 5.1. Since the stochastic process of the velocity u in space x does not have the exact Markov property (see Chapter 3), the direct modeling of $u(x)$ as a Markov process is not an exact method to obtain a stochastic mulit-point description of turbulence. Nevertheless, it might well be of interest for the practical purpose of modeling turbulence in computational fluid dynamics.

On the other hand, the stochastic cascade process of velocity increments does have the Markov property, and the exact multi-scale statistics of homogeneous turbulence can be obtained by this method. However, in this approach, the actual values of the velocity are somehow filtered out, and the multi-point statistics can not be derived straightforward from the multi-scale statistics. In Chapter 4, we show how this method can be extend in order to obtain the complete multi-point statistics of the turbulent velocity, given by the joint PDF $p[u(x_1), u(x_2), \ldots, u(x_N)]$ of the velocities at N points x_n. We show how

this N-point PDF can be expressed by three-point PDFs of the velocity field, and propose a stochastic three-point closure for the velocity field of homogeneous isotropic turbulence.

Bibliography

[1] A. N. Kolmogorov. The local structure of turbulence in incompressible viscous fluid for very high Reynolds numbers. *Dokl. Acad. Nauk SSSR*, 30:299–303, 1941, english version in: *Proc. R. Soc. Lond. A*, 434:9–13, 1991.

[2] A. N. Kolmogorov. On degeneration of isotropic turbulence in an incompressible viscous fluid. *Dokl. Akad. Nauk SSSR*, 31:538–541, 1941.

[3] A. N. Kolmogorov. Dissipation of energy in locally isotropic turbulence. *Dokl. Akad. Nauk SSSR*, 32:16–18, 1941, english version in: *Proc. R. Soc. Lond. A*, 434:15–17, 1991.

[4] K. R. Sreenivasan and R. A. Antonia. The phenomenology of small-scale turbulence. *Annu. Rev. Fluid Mech.*, 29:435–472, 1997.

[5] L. F. Richardson. *Weather Prediction by Numerical Process*. Cambridge University Press, 1922.

[6] U. Frisch. *Turbulence – The legacy of A. N. Kolmogorov*. Cambridge University Press, 1995.

[7] G. I. Taylor. Statistical theory of turbulence. *Proc. R. Soc. London*, 151:421–444, 1935.

[8] G. K. Batchelor. *The Theory of Homogeneous Turbulence*. Cambridge University Press, 1953.

[9] K. R. Sreenivasan. On the scaling of the turbulent energy dissipation rate. *Phys. Fluids*, 27:1048–1051, 1984.

[10] K. R. Sreenivasan. An update on the energy dissipation rate in isotropic turbulence. *Phys. Fluids*, 10:528, 1998.

[11] Y. Kaneda, T. Ishihara, M. Yokokawa, K. Itakura, and A. Uno. Energy dissipation rate and energy spectrum in high resolution direct numerical simulations of turbulence in a periodic box. *Phys. Fluids*, 15:L21, 2003.

[12] P. Burattini, Pl Lavoie, and R. A. Antonia. On the normalized turbulent energy dissipation rate. *Phys. Fluids*, 17:098103, 2005.

[13] A. N. Kolmogorov. A refinement of previous hypotheses concerning the local structure of turbulence in a viscous incompressible fluid at high Reynolds number. *J. Fluid Mech.*, 13:82–85, 1962.

[14] D. Hurst and J. C. Vassilicos. Scalings and dacay of fractal-generated turbulence. *Phys. Fluids*, 19:035103, 2007.

[15] R. E. Seoud and J. C. Vassilicos. Dissipation and decay of fractal-generated turbulence. *Phys. Fluids*, 19:105108, 2007.

[16] N. Mazellier and J. C. Vassilicos. The turbulece dissipation constant is not universal because of its universal dependence on large-scale flow topology. *Phys. Fluids*, 20:015101, 2008.

[17] R. E. Seoud and J. C. Vassilicos. Fully developed turbulence with diminishing mean vortex stretching and reduced intermittency. In J. Peinke, M. Oberlack, and A. Talamelli, editors, *Progress in Turbulence III – Proceedings of the iTi Conference in Turbulence 2008*, pages 1–8. Springer Verlag, 2009.

[18] C. W. van Atta and R. A. Antonia. Reynolds number dependence of skewness and flatness factors of turbulent velocity derivatives. *Phys. Fluids*, 23:252–257, 1980.

[19] C. L. Fefferman. Existence and smoothness of the Navier–Stokes equation. http://www.claymath.org/millennium/Navier-Stokes_Equations/.

[20] G. Comte-Bellot and S. Corrsin. The use of a contraction to improve the isotropy of grid-generated turbulence. *J. Fluid. Mech.*, 25:657, 1966.

[21] W. K. George. The decay of homogeneous isotropic turbulence. *Phys. Fluids A*, 4:1492, 1992.

[22] W. K. George and H. Wang. The exponential decay of homogeneous turbulence. *Phys. Fluids*, 19:025108, 2007.

[23] M. Oberlack and G. Khujadze. Fractal-generated turbulent scaling laws from a new scaling group of the multi-point correlation equation. In J. Peinke, M. Oberlack, and A. Talamelli, editors, *Progress in Turbulence III – Proceedings of the iTi Conference in Turbulence 2008*, pages 13–19. Springer Verlag, 2009.

[24] H. Risken. *The Fokker-Planck Equation*. Springer Verlag, 1996.

[25] R. Friedrich and J. Peinke. Description of a turbulent cascade by a Fokker-Planck equation. *Phys. Rev. Lett.*, 78:863–866, 1997.

[26] R. Friedrich and J. Peinke. Statistical properties of a turbulent cascade. *Physica D*, 102:147–155, 1997.

[27] R. Friedrich, J. Zeller, and J. Peinke. A note on three-point statistics of velocity increments in turbulence. *Europhys. Lett.*, 41:153–158, 1998.

[28] C. Renner, J. Peinke, and R. Friedrich. Experimental indications for Markov properties of small-scale turbulence. *J. Fluid Mech.*, 433:383–409, 2001.

[29] C. Renner, J. Peinke, R. Friedrich, O. Chanal, and B. Chabaud. Universality of small scale turbulence. *Phys. Rev. Lett.*, 89: 124502, 2002.

[30] M. Tutkun and L. Mydlarski. Markovian properties of passive scalar increments in grid-generated turbulence. *New J. Phys.*, 6: 49, 2004.

[31] M. Siefert and J. Peinke. Different cascade speed for longitudinal and transverse velocity increments of small-scale turbulence. *Phys. Rev. E*, 70:015302, 2004.

[32] M. Siefert and J. Peinke. Joint multi-scale statistics of longitudinal and transversal increments in small-scale wake turbulence. *J. Turb.*, 7:1–35, 2006.

[33] M. Wächter, F. Riess, H. Kantz, and J. Peinke. Stochastic analysis of surface roughness. *Europhys. Lett.*, 64:579–585, 2003.

[34] G. R. Jafari, S. M. Fazeli, F. Ghasemi, S. V. Allaei, M. R. R. Tabar, A. I. Zad, and G. Kavei. Stochastic analysis and regeneration of rough surfaces. *Phys. Rev. Lett.*, 91:226101, 2003.

[35] P. Manshour, S. Saberi, M. Sahimi, J. Peinke, A. F. Pacheco, and M. R. R. Tabar. Turbulencelike behavior of seismic time series. *Phys. Rev. Lett.*, 102:014101, 2009.

[36] C. Renner, J. Peinke, and R. Friedrich. Evidence of Markov properties of high frequency exchange rate data. *Physica A*, 298:499–520, 2001.

[37] M. Ausloos and K. Ivanova. Dynamical model and nonextensive statistical mechanics of a market index on large time windows. *Phys. Rev. E*, 68, 2003.

[38] A. P. Nawroth and J. Peinke. Medium and small scale analysis of financial data. *Physica A*, 382:193, 2007.

[39] S. Lück, C. Renner, J. Peinke, and R. Friedrich. The Markov–Einstein cohernce length—a new meaning for the Taylor length in turbulence. *Phys. Lett. A*, 359:335–338, 2006.

[40] M. Wächter, A. Kouzmitchev, and J. Peinke. Increment definitions for scale-dependent analysis of stochastic data. *Phys. Rev. E*, 70: 055103, 2004.

[41] D. Kleinhans. *Stochastische Modellierung komplexer Systeme*. PhD thesis, Universität Münster, Münster, Germany, 2008.

[42] R. H. Kirchhoff, F. C. Kaminsky, and C. Y. Syu. Synthesis of wind speed using a markov chain. In *Eighth ASME Wind Energy Symposium*, 1989.

[43] F. C. Kaminsky, R. H. Kirchhoff, C. Y. Syu, and J. F. Manwell. A comparison of alternative approaches for the synthetic generation of a wind speed time series. *J. Sol. Energy Eng.*, 113:280–289, 1991.

[44] A. S. Monin and A. M. Yaglom. *Statistical Fluid Mechanics: Mechanics of Turbulence*, volume 1. The MIT Press, 1975.

Chapter 2

Fractal-generated turbulence – Defining a new class of turbulent flows[1]

Abstract We apply a method based on the theory of Markov processes to fractal-generated turbulence and obtain joint probabilities of velocity increments at several scales. From experimental data we extract a Fokker-Planck equation which describes the interscale dynamics of the turbulence. In stark contrast to all documented boundary-free turbulent flows, the multiscale statistics of velocity increments, the coefficients of the Fokker-Planck equation, and dissipation-range intermittency are all independent of R_λ (the characteristic ratio of inertial to viscous forces in the fluid). These properties define a qualitatively new class of turbulence.

[1] Published as R. STRESING, J. PEINKE, R. E. SEOUD, and J. C. VASSILICOS: Defining a new class of turbulent flows, *Phys. Rev. Lett.* **104**, 194501, 2010.

2.1 Introduction

Recent experimental observations of fluid flow turbulence generated by fractal grids like the one shown in Fig. 2.1 have revealed some remarkable properties. Turbulence generated by space-filling fractal square grids is homogeneous and isotropic far enough downstream where it freely decays *exponentially* and *not* as a power law as is the case in all previously well-documented boundary-free turbulent flows (regular grid turbulence, wakes, jets, etc.) [1, 2]. As predicted by a theoretical study [3], this exponentially decaying turbulence is locked into a single length-scale, meaning that the inner Taylor microscale λ and the outer integral length scale L are both proportional to it. As a result, the ratio L/λ stays constant during decay, although the Reynolds number changes [4]. This implies an independence of the ratio of outer to inner length scales L/λ on Reynolds number which means that fractal-generated homogeneous isotropic turbulence is fundamentally incompatible with the usual Richardson-Kolmogorov cascade picture of small-scale turbulence dynamics where, as the Reynolds number increases, the range of scales needed for the turbulence energy to cascade down to scales small enough for dissipation to occur, also increases. In other words, a wider range of length-scales is needed for the Richardson-Kolmogorov cascade to cause turbulence to dissipate at higher Reynolds numbers. Indeed, L/λ is proportional to, and therefore increases with, the Taylor length-based Reynolds number R_λ in all boundary-free turbulent flows [2, 5] which are not fractal generated.

Standard statistical analysis of small-sale turbulence is based on two-point correlations and their dependence on the distance r between the two points. A central quantity is the longitudinal velocity increment $\xi(r)$,

$$\xi(r) = u(x+r) - u(x), \tag{2.1}$$

where u denotes the fluctuating velocity component in the direction defined by two points x and $x+r$. As mentioned above and shown in [3, 4], fractal-generated turbulence can be such that $\langle \xi(r)^2 \rangle = u_{\mathrm{rms}}^2 f(r/l)$ where the brackets $\langle ... \rangle$ denote an averaging operation, u_{rms} is the rms of $u(x)$, f is a dimensionless function and l is a single length scale determined by the fractal grid, independent of R_λ and such that $L \sim l$ and $\lambda \sim l$. This self-preserving form of the second-order structure function is qualitatively very different from the basic Kolmogorov scaling

$\langle \xi(r)^2 \rangle = u_{\rm rms}^2 f(r/L, r/\eta) = u_{\rm rms}^2 g(r/L, L/\eta)$ where f and g are dimensionless functions, η is the Kolmogorov microscale and $L/\eta \sim R_\lambda^{3/2}$ (equivalently $L/\lambda \sim R_\lambda$). This Kolmogorov scaling involves two different length-scales, one outer (L) and one inner (η or λ), and is based on the Richardson-Kolmogorov phenomenology which also requires that $g(r/L) \sim (r/L)^{2/3}$ in the intermediate asymptotic range $\eta \ll r \ll L$ as $L/\eta \to \infty$, so that $\langle \xi(r)^2 \rangle \sim (\varepsilon r)^{2/3}$ in that range with $\varepsilon \sim u_{rms}^3/L$.

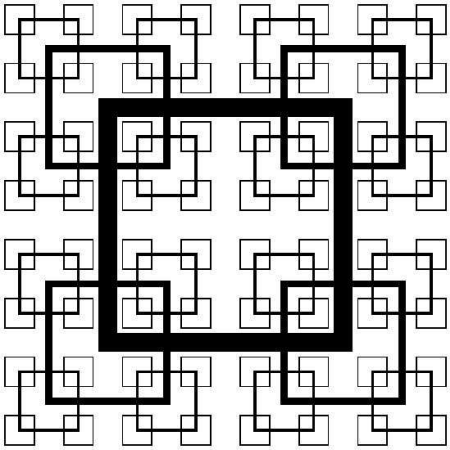

Figure 2.1: Fractal square grid.

These exceptional properties of fractal-generated turbulence, in particular the apparent absence of a conventional Richardson-Kolmogorov cascade, call for a deeper analysis of its multiscale structure. The study of all structure functions $\langle \xi(r)^n \rangle$ is equivalent to the study of the probability density functions (PDF) $p[\xi(r)]$. Such a study can reveal whether it is in fact $p[\xi(r)]$ which is self-preserving and independent of R_λ or whether it has a Kolmogorov two-scale (inner and outer) dependence and therefore depends on R_λ. However, as there are infinite different possible interscale processes to generate the same one scale $p(\xi)$ statistics, a full multiscale characterization is needed in terms of the multiscale PDF $p(\xi_0, \xi_1, ..., \xi_M)$ where $\xi_m \equiv \xi(r_m)$ for $m = 0, 1, ..., M$. This multiscale PDF is the joint probability of finding velocity increments on several scales and goes beyond the traditional analysis based on structure functions as $p[\xi(r)]$ can be deduced by integrations. Here we study

this multiscale PDF for the purpose of achieving a most general differentiation between fractal-generated turbulence and other boundary-free turbulent flows.

The analysis we use gives access to the multiscale PDF $p(\xi_0, \xi_1, ..., \xi_M)$ by characterizing the underlying stochastic interscale process in the form of a Fokker-Planck equation. If the stochastic process for the evolution of the velocity increments from scale to scale ($r_M < r_{M-1} < ... < r_0$) has Markov properties, i.e. if

$$p(\xi_M|\xi_{M-1}, ..., \xi_0) = p(\xi_M|\xi_{M-1}), \tag{2.2}$$

the multiscale PDF $p(\xi_M, ..., \xi_1, \xi_0)$ can be expressed by a product of conditional PDFs $p(\xi_m|\xi_{m-1})$. The stochastic process for these conditional PDFs can be described by a Kramers-Moyal expansion. If the fourth-order Kramers-Moyal coefficient $D^{(4)}$ is zero, the expansion truncates after the second term (Pawula's theorem) and becomes a Fokker-Planck equation:

$$-\frac{\partial}{\partial r}p(\xi|\xi_0) = -\frac{\partial}{\partial \xi}\left[D^{(1)}(\xi, r)p(\xi|\xi_0)\right] + \frac{\partial^2}{\partial \xi^2}\left[D^{(2)}(\xi, r)p(\xi|\xi_0)\right], \tag{2.3}$$

where for simplicity we use the notations $\xi \equiv \xi(r)$ and $\xi_0 \equiv \xi(r_0)$ with $r < r_0$. The drift and diffusion functions $D^{(1)}$ and $D^{(2)}$ can be estimated as Kramers-Moyal coefficients pointwise by:

$$D^{(k)}(\xi, r) = \lim_{\Delta r \to 0} \frac{r}{k!\Delta r} \int_{-\infty}^{+\infty} (\tilde{\xi} - \xi)^k \, p[\tilde{\xi}(r - \Delta r)|\xi(r)] \, \mathrm{d}\tilde{\xi}. \tag{2.4}$$

It has been shown for several different flows [6, 7, 8, 9, 10] that (a) the process has Markov properties, (b) $D^{(4)}$ vanishes or is small enough to be neglected, and (c) the experimental (conditional) PDFs of the velocity increments can be reproduced by integration of the Fokker-Planck equation, including intermittency effects.

2.2 Experimental results

We analyze hot-wire measurement data from turbulence generated in a wind tunnel by a fractal square grid shown schematically in Fig. 2.1. The design of this grid is space filling in the sense that the fractal dimension D_f of the line defined by all the bars without their thickness takes the maximum value 2. The spanwise thickness of these bars determines the blockage ratio independently of the value of D_f, and it is 25% here, which is small compared to regular and active grids. The ratio of the thicknesses of the largest to that of the smallest bars of the grid is $t_r = 17$ [11]. Measurements are taken for two different flow velocities at five different downstream positions in the decay region, where the turbulence is small-scale homogeneous and isotropic [4]. For comparison, we use results from [8, 9] for hot-wire measurements of the streamwise velocity component along the center line of a cryogenic free jet, as well as new results from the analysis of hot-wire measurements of the streamwise velocity component in the center of the wake of a cylinder with diameter D = 2 cm at downstream-distance $x = 100$ D.

For the fractal grid data we confirm the result of [4] that λ is almost independent of downstream position. We find that the stochastic process for the velocity increments has Markov properties for scale separations $\Delta r \equiv r_{m-1} - r_m$ greater than the *Einstein-Markov coherence length* l_{EM}, which is defined as the smallest Δr for which Eq. (2.2) holds. We estimate l_{EM} with the (Mann-Whitney-)Wilcoxon test, which tests the validity of the equation $p(\xi_2|\xi_1,\xi_0) = p(\xi_2|\xi_1)$ for different values of Δr (cf. [8]). For the fractal grid data, we find a constant ratio of $l_{EM}/\lambda = 0.73 \pm 0.09$, which is comparable to previous results for other turbulent flows, where $l_{EM}/\lambda \approx 0.8$ [7].

We determine the Kramers-Moyal coefficients with two different methods. The first method directly uses definition (2.4), determining the limit of $\Delta r \to 0$ with a linear fit to the conditional moments on the right hand side of Eq. (2.4) in the range $l_{EM} \leq \Delta r \leq 2l_{EM}$, following [8, 9]. The drift and diffusion functions at each scale r can then be approximated by linear and second-order functions in ξ, respectively:

$$D^{(1)}(\xi, r) = -d_{11}(r)\xi, \tag{2.5}$$

$$D^{(2)}(\xi, r) = d_{20}(r) - d_{21}(r)\xi + d_{22}(r)\xi^2. \tag{2.6}$$

The second method uses numerical optimization to find the optimal coefficients $d_{ij}(r)$ of Eq. (2.5) and (2.6). Here, the Kullback-Leibler en-

tropy is used to minimize the distance between the empirical conditional PDF $p(\xi_m|\xi_{m-1})$, and the conditional PDF obtained by numerical integration of the Fokker-Planck equation (2.3) [12]. Both the direct and optimization methods lead to consistent results.

The velocity increments $\xi(r)$ are given in units of their standard deviation in the limit $r \to \infty$, σ_∞, which is identical to $\sqrt{2}$ times the standard deviation σ_u of the velocity u [8]. This normalization allows us to compare the Kramers-Moyal coefficients of different flows.

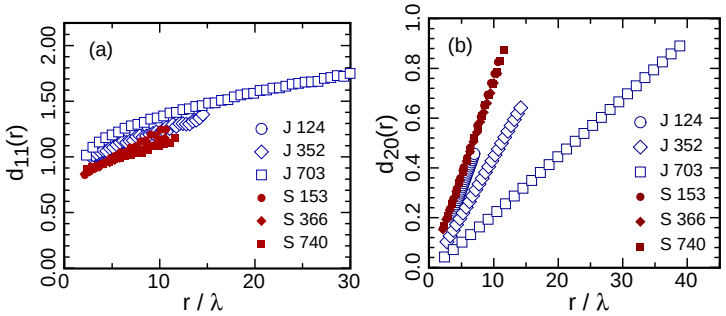

Figure 2.2: Coefficients d_{11} (a) and d_{20} (b) as functions of the scale r for the free jet (J), from [9], and fractal square grid (S). Reynolds numbers R_λ are given in the legends.

Fig. 2.2(a) shows that the coefficient d_{11} has a similar dependence on r for the fractal grid as for the free jet, and does not depend significantly on the Reynolds number for both flows. In contrast, the coefficient d_{20} does depend strongly on R_λ for the free jet [8, 9], but not for the fractal grid, as can be seen in Fig. 2.2 (b). The coefficient d_{20} is linear in r and thus can be approximated by

$$d_{20}(r) = d_{20}^* \frac{r}{\lambda}. \tag{2.7}$$

As shown in Fig. 2.3, d_{20}^* follows a power law in R_λ for the free jet [9], as well as for the cylinder wake data where the exponent seems to be smaller. In contrast, the slope d_{20}^* is approximately constant for fractal grid turbulence. For both d_{11} and d_{20}, the optimized coefficients differ only slightly from the ones estimated by the classical method.

Renner *et al.* [8, 9] also find a strong R_λ dependence of the coefficients d_{21} and d_{22} for free-jet data. For the fractal grid, we find no

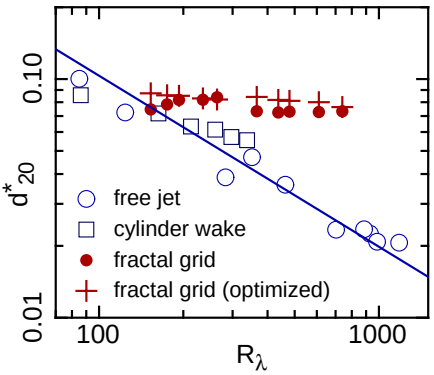

Figure 2.3: Slopes d_{20}^* from Eq. (2.7) as functions of R_λ for the free jet, cylinder wake, and fractal grid. The free-jet data are taken from [9]. The straight line represents a power law $d_{20}^* = 2.8Re^{3/8}$ from [9], where $R_\lambda \approx Re^{1/2}$.

systematic dependence on R_λ for the optimized values of these coefficients.

As an alternative and independent verification of the Reynolds number independence of the statistical properties of fractal grid turbulence we now investigate the conditional PDFs $p(\xi|\xi_0)$, where $r \ll r_0$. Note that these are the fundamental quantities which contain the information of the stochastic process integrated over a range of scales. Most importantly, the conditional PDFs do not contain the errors and uncertainties which arise in estimating the Kramers-Moyal coefficients.

Fig. 2.4 shows the conditional PDFs $p(\xi|\xi_0)$, as well as the PDFs $p(\xi)$, which are obtained by integration over ξ_0, for $r = 3l_{EM}$ and $r_0 = 9l_{EM}$, for the fractal grid, free jet, and cylinder wake. The PDFs for high and low Reynolds numbers are plotted into the same graph for comparison.

The (conditional) PDFs of the fractal grid data in Fig. 2.4(a) are practically identical at different Reynolds numbers. The small deviations in the tails of the distributions can be attributed to statistical errors due to the small number of events in the corresponding bins. In contrast to this, the (conditional) PDFs of the free jet and cylinder wake data in Fig. 2.4(b) and 2.4(c), respectively, exhibit large differences for

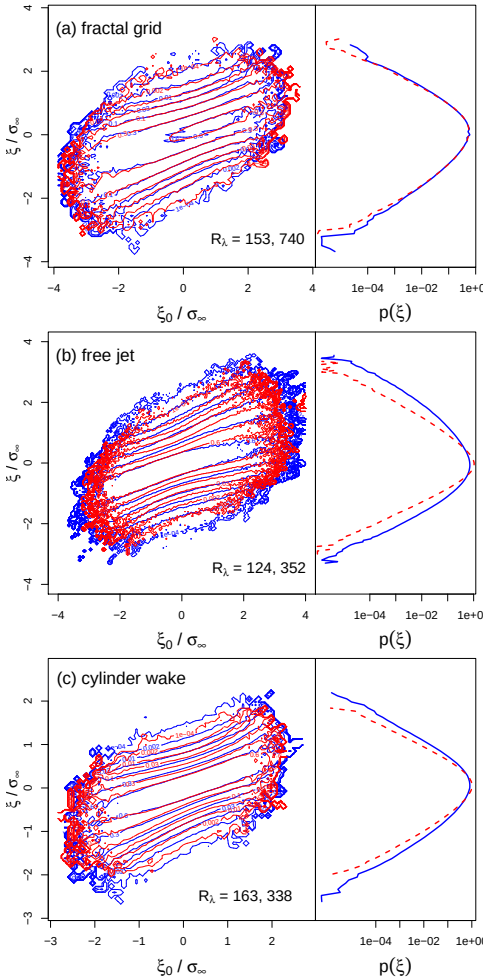

Figure 2.4: Conditional PDFs $p[\xi(r)|\xi(r_0)]$ (left), and PDFs $p[\xi(r)]$ (right, rotated by 90° to illustrate the relation to the plots on the left), for $r = 3l_{EM}$ and $r_0 = 9l_{EM}$. (a) fractal grid, $R_\lambda = 153$ (solid), 740 (dashed). (b) free jet, $R_\lambda = 124$ (solid) 352 (dashed). (c) cylinder wake, $R_\lambda = 163$ (solid), 338 (dashed).

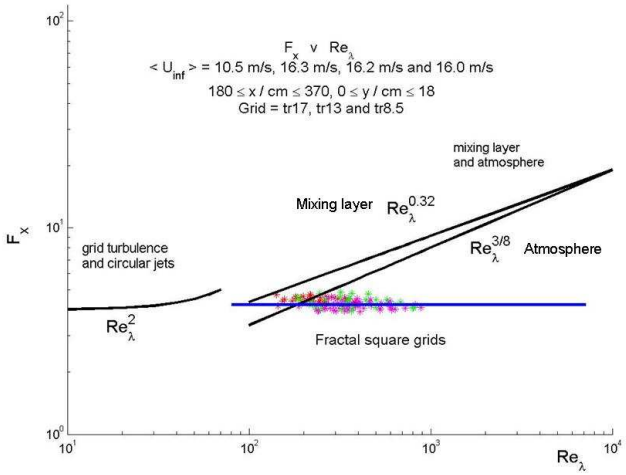

Figure 2.5: Flatness $F_x = \langle u_x^4 \rangle / \langle u_x^2 \rangle^2$ of the velocity derivatives $u_x = \partial u / \partial x$ for different fractal square grids in comparison to other types of turbulence.

different Reynolds numbers.

The conditional PDFs $p(\xi|\xi_0)$ characterize the interscale dynamics of the small-scale turbulence. Our results strongly suggest that there is a qualitative difference between the interscale dynamics of turbulence generated by space-filling fractal square grids and the interscale dynamics of other boundary-free turbulence such as jet and wake turbulence. The conditional PDFs $p(\xi|\xi_0)$ of our fractal-generated turbulence do not depend on Reynolds number whereas those of other turbulent flows do. This is probably the most fundamental way in which these two different classes of turbulence differ. A particular consequence of the Reynolds number independence of $p(\xi|\xi_0)$ is the Reynolds number independence of $p(\xi)$ which is obtained by integrating $p(\xi|\xi_0)$ over ξ_0. This is confirmed by the right plots of Fig. 2.4 where it is also shown that $p(\xi)$ is R_λ-dependent in jet and wake turbulence.

The method of stochastic analysis applied in this Letter is limited to scales r larger than the Einstein-Markov length l_{EM} ($\approx \lambda$) and

therefore so are our conclusions concerning $p(\xi|\xi_0)$. However, if we allow ourselves to extrapolate the Reynolds number independence of $p[\xi(r)]$ to all scales r, then our fractal-generated turbulence is incompatible with Kolmogorov scaling $\langle \xi(r)^n \rangle = u_{\rm rms}^2 g_n(r/L, L/\eta)$ (where $L/\eta \sim R_\lambda^{3/2}$) and must instead obey self-preserving single-length-scale forms $\langle \xi(r)^n \rangle = u_{\rm rms}^n f_n(r/l)$ as previously reported for $n = 2$ [3, 4].

The second remarkable consequence of such an extrapolated Reynolds number independence of $p[\xi(r)]$ is the absence of Reynolds number dependent dissipation-range intermittency, unlike all documented flows (see [1, 13]). Our data strongly support this conclusion. Fig. 2.5 is a plot of the derivative flatness F_x; it is clear that it does not depend on R_λ, in very stark contrast with all other documented turbulent flows where F_x grows with R_λ [13].

2.3 Conclusions

Homogeneous and isotropic small-scale turbulence generated by a low-blockage space-filling fractal square grid (Fig. 2.1) is similar to other boundary-free turbulent flows in that the stochastic process for the evolution of the velocity increments from scale to scale has Markov properties for scale separations greater than the Taylor microscale λ. However, this fractal-generated turbulence differs qualitatively from other documented boundary-free turbulent flows [1, 8, 9, 13] in that the resulting drift and diffusion functions (2.5) and (2.6) and the multiscale joint probability functions which they determine are all independent of R_λ. The single-scale probability density function of velocity increments is also independent of R_λ. This implies the absence of (inner and outer) Kolmogorov scaling and of R_λ-dependent dissipation-range intermittency. These properties are in stark contrast with all documented turbulent flows [1, 8, 9, 13]. Thus we believe we have found a qualitatively new class of fluid flow turbulence.

These findings have significant implications for the issue of universality and pave the way for hitherto inconceivable studies on the very conditions which allow the Richardson-Kolmogorov cascade to hold or not, over and above the intermittency corrections usually studied.

We thank C. Renner, O. Chanal, and B. Chabaud for the free-jet data, and S. Lück for the cylinder wake data. We acknowledge support from DFG Grant No. PE 478/14-1 and from EPSRC GR/S23293.

Bibliography

[1] U. Frisch. *Turbulence – The legacy of A. N. Kolmogorov*. Cambridge University Press, 1995.

[2] H. Tennekes and J. L. Lumley. *A first course in turbulence*. MIT Press, 1972.

[3] W. K. George and H. Wang. The exponential decay of homogeneous turbulence. *Phys. Fluids*, 19:025108, 2007.

[4] R. E. Seoud and J. C. Vassilicos. Dissipation and decay of fractal-generated turbulence. *Phys. Fluids*, 19:105108, 2007.

[5] S. B. Pope. *Turbulent Flows*. Cambridge University Press, 2000.

[6] R. Friedrich and J. Peinke. Description of a turbulent cascade by a Fokker-Planck equation. *Phys. Rev. Lett.*, 78:863–866, 1997.

[7] S. Lück, C. Renner, J. Peinke, and R. Friedrich. The Markov–Einstein cohernce length—a new meaning for the Taylor length in turbulence. *Phys. Lett. A*, 359:335–338, 2006.

[8] C. Renner, J. Peinke, and R. Friedrich. Experimental indications for Markov properties of small-scale turbulence. *J. Fluid Mech.*, 433:383–409, 2001.

[9] C. Renner, J. Peinke, R. Friedrich, O. Chanal, and B. Chabaud. Universality of small scale turbulence. *Phys. Rev. Lett.*, 89:124502, 2002.

[10] M. Tutkun and L. Mydlarski. Markovian properties of passive scalar increments in grid-generated turbulence. *New J. Phys.*, 6:49, 2004.

[11] D. Hurst and J. C. Vassilicos. Scalings and dacay of fractal-generated turbulence. *Phys. Fluids*, 19:035103, 2007.

[12] A. P. Nawroth, J. Peinke, D. Kleinhans, and R. Friedrich. Improved estimation of Fokker-Planck equations through optimisation. *Phys. Rev. E*, 76:056102, 2007.

[13] K. R. Sreenivasan and R. A. Antonia. The phenomenology of small-scale turbulence. *Annu. Rev. Fluid Mech.*, 29:435–472, 1997.

Chapter 3

Markov properties of turbulence[1]

Abstract We study the Markov property of experimental velocity data of different homogeneous isotropic turbulent flows. In particular, we examine the stochastic "cascade" process of nested velocity increments $\xi(r) := u(x+r) - u(x)$ as a function of scale r for different nesting structures. It was found in previous work that for a certain nesting structure, the stochastic process of $\xi(r)$ has the Markov property for step sizes larger than the so-called *Einstein-Markov coherence length* l_{EM}, which is of the order of magnitude of the Taylor microscale λ [1]. We now show that if a reasonable definition of the effective step size of the process is applied, this result holds independently of the nesting structure. Furthermore, we analyze the stochastic process of the velocity u as a function of the spatial position x. Although this process does not have the exact Markov property, a characteristic length scale $l_{u(x)} \approx l_{EM}$ can be identified on the basis of a statistical test for the Markov property. Using a method based on the matrix of transition probabilities, we examine the significance of the non-Markovian character of the velocity $u(x)$ for the statistical properties of turbulence.

[1] Submitted to *Phys. Rev. E* as R. STRESING, D. KLEINHANS, R. FRIEDRICH, and J. PEINKE: Different methods to estimate the Einstein-Markov coherence length in turbulence.

3.1 Introduction

Complex systems are often characterized by hierarchical structures at different scales, which can frequently be described in terms of scale-dependent quantities which obey stochastic differential equations. Examples of complex systems that have been successfully described by stochastic processes in scale are turbulence [1, 2, 3, 4, 5, 6, 7, 8], roughness of surfaces [9, 10], eathquakes [11], and financial data [12, 13, 14]. In all cases, the analysis is greatly simplified by the assumption that the corresponding stochastic process has the Markov property.

For most real-world phenomena, however, the assumption of the Markov property must be limited to large enough step sizes of the stochastic processes. To our knowledge, this has first been recognized by Einstein for Brownian motion of particles suspended in a fluid [15]. Einstein discussed a smallest time scale from which on the Brownian motion of a dispersed particle can be described by a Markovian stochastic process, since the stochastic forcing decorrelates. We call the spatial equivalent of this time scale the *Einstein-Markov coherence length*, l_{EM}.

If a complex system can be described by a Markovian stochastic process in scale this has an important implication: the multi-scale statistics, and eventually also the multi-point statistics of the system can be expressed as a product of three-point statistics [8]. Therefore, the complexity of the system is greatly reduced in presence of the Markov property. Furthermore, the Einstein-Markov length contains relevant information about the dynamics of the system. For example, it has been found that the Einstein-Markov length of seismic data increases significantly before the occurrence of a major earthquake, indicating that the statistical coherence of the system increases before such a large-scale event takes place [16]. For homogeneous isotropic turbulence, the Einstein-Markov length of the stochastic process in scale is of the order of magnitude of the Taylor microscale λ, thus giving a new interpretation to this important length scale [1].

Given the fundamental importance of the Einstein-Markov coherence length for the statistical analysis of complex systems in general, and turbulence in particular, in the present paper we have a closer look at the Markov property of a scale-dependent variable ξ as a function of scale r. Furthermore, we extend the analysis to the stochastic process of the local velocity u as a function of spatial position x.

Note that the series of velocity data $u(x)$ are actually obtained from

time series of velocity values $u(t)$ measured at a fixed position x_0 in the turbulent flow. This is done by using Taylor's "frozen turbulence" hypothesis, which states that the turbulent velocity field does not change significantly at small scales while it sweeps over the sensor with the mean flow velocity $\overline{u}$. Therefore, time lags Δt can be transformed into spatial distances Δx by assuming that $\Delta x = \overline{u} \cdot \Delta t$. Taylor's hypothesis is widely used in turbulence research as an approximation for small turbulence intensity $\sigma_u/\overline{u} \ll 1$, where $\sigma_u = \sqrt{\langle (u-\overline{u})^2 \rangle}$ (e.g. [17]).

The most common scale-dependent measure of the turbulent velocity field is the velocity increment. The (longitudinal) velocity increment ξ at the point x and scale r is defined as

$$\xi(x,r) = u(x+[1-q]r) - u(x-qr), \tag{3.1}$$

where $u(x')$ is the streamwise velocity at point x'. The parameter $q \in [0,1]$ defines the nesting structure of velocity increments at two or more scales $r_1, r_2, \ldots$. The special cases of $q = 0$, 1/2, and 1 will be called left-bounded, centered, and right-bounded velocity increments, respectively.

We now consider the statistics of $\xi(r,x)$ as a function of the scale r. The process $\xi(r)$ has the Markov property, if

$$p[\xi(r_1)|\xi(r_2),\xi(r_3),\ldots,\xi(r_N)] = p[\xi(r_1)|\xi(r_2)], \tag{3.2}$$

where we assume that $r_1 < r_2 < \ldots < r_N$. If (3.2) holds, the N-scale joint probability density function (PDF) $p[\xi(r_1),\xi(r_2),\ldots,\xi(r_N)]$ factorizes into a product of simple conditional PDFs,

$$\begin{aligned} p[\xi(r_1),\xi(r_2),\ldots,\xi(r_N)] = \\ p[\xi(r_1)|\xi(r_2)] \ldots p[\xi(r_{N-1})|\xi(r_N)] \cdot p[\xi(r_N)]. \end{aligned} \tag{3.3}$$

The evolution of the conditional PDFs in scale r then can be described by a Kramers-Moyal expansion [2, 18]. Under certain conditions which can be verified during analysis (the coefficient of fourth order, $D^{(4)}$, has to vanish) the expansion reduces to a Fokker-Planck equation,

$$\begin{aligned} -r\frac{\partial}{\partial r} p[\xi(r)|\xi'(r')] = &-\frac{\partial}{\partial \xi}\left[D^{(1)}(\xi,r)\, p[\xi(r)|\xi'(r')]\right] \\ &+\frac{\partial^2}{\partial \xi^2}\left[D^{(2)}(\xi,r)\, p[\xi(r)|\xi'(r')]\right], \end{aligned} \tag{3.4}$$

where we request $r' > r$, which implies a direction of the process from large to small scales [2, 18]. $D^{(1)}(\xi, r)$ and $D^{(2)}(\xi, r)$ are the drift and diffusion function, respectively.

As shown in [1, 2, 3, 4, 5] for left-bounded velocity increments of homogeneous isotropic turbulence, the process of $\xi(r)$ has the Markov property if the difference between the scales, $\Delta r = r_i - r_{i-1}$, is larger than $l_{EM} \approx \lambda$. It has also been demonstrated that the fourth-order Kramers-Moyal coefficient in fact can be neglected [4, 6] and thus, the stochastic interscale process can be described by a Fokker-Planck equation. The scale-dependent drift and diffusion functions can be estimated directly from the data [4, 5] or obtained from an iterative numerical optimization procedure [19].

This analysis provides access to the N-scale statistics of homogeneous isotropic turbulence, including a correct reconstruction of the so-called structure functions $\langle \xi(r)^n \rangle$. If, additionally, the dependence of the drift and diffusion functions on the velocity u is taken into account, the N-point statistics $p[u(x_1), u(x_2), \ldots, u(x_N)]$ can also be obtained [8]. Thus, a complete statistical characterization of the turbulent velocity based on a stochastic three-point closure is achieved.

The remaining part of the paper is organized as follows: In Section 3.2.1, we briefly describe the experimental data. In Section 3.2.2, we examine the influence of the nesting parameter q in (3.1) on the Markov property of the process of the velocity increment ξ as a function of scale r. In Section 3.2.3, we examine the Markov property of the stochastic process of the velocity u as a function of spatial position x. In Section 3.3, we generate synthetic data from the empirical transition matrices of measured velocity data, and investigate which statistical properties of turbulence can be reproduced by such a Markovian model. Section 3.4 concludes this paper.

3.2 Markov properties

3.2.1 Experimental data

We analyze seven data sets from four different experimental setups in order to cover a wide range of Reynolds numbers for different flow types. All data has been measured with hot-wire probes with a single wire or a cross-wire. In the latter case, we examine the streamwise

velocity component.

We use data measured in the center of an axisymmetric air free jet at 145 nozzle-diameters distance from the nozzle, at a Taylor-based Reynolds-number of R_λ = 190 [4], and data measured in the center of a cryogenic helium gas free jet with a temperature close to 4 K at 40 nozzle-diameters distance from the nozzle at R_λ = 124 and R_λ = 352 [20]. These data have already been analyzed in great detail in [4, 5, 1].

We also analyze data measured in the center of the wake of a cylinder with diameter D = 2 cm at downstream-distance $x = 100$ D, at R_λ = 163 and R_λ = 338 [21].

Furthermore, we use data measured in the decay region of the air flow behind a fractal square grid with the fractal dimension D_f = 2, a blockage ratio of 25% and a thickness ratio of the thickest to the thinnest bars of the grid of t_r = 17, described in detail in [22].

3.2.2 Markov property of the interscale process $\xi(r)$

First, we examine the influence of the nesting structure of the velocity increments on the Markov property of the stochastic process of ξ as a function of scale r. This analysis is motivated by the results of [23, 24] suggesting that left-bounded velocity increments, i.e. a nesting parameter of $q = 0$ in (3.1), introduce spurious correlations which also affect the Markov property [23], and which do not occur for centered velocity increments with $q = 1/2$. Since almost all previous studies of interscale dynamics were based on left-bounded increments, it might be needed to consider to shift the scope of the analysis to centered velocity increments in order to avoid spurious correlations. However, before doing so, one should examine more closely how the nesting parameter q affects the Markov property and the Einstein-Markov coherence length of the process. This will be done in the present section.

When examining the Markov property of measured data, we focus on the case of $N = 3$ in (3.2), because the amount of data typically is not sufficient to test more than two conditions on the left hand side of the equation. Moreover, processes where the statistics of the stochastic variable Y_i depend on Y_{i-1} and Y_{i-3} but *not* on Y_{i-2}, would be rather special and are not to be expected in natural phenomena like turbulence [2]. Thus (3.2) simplifies to

$$p[\xi(r_1)|\xi(r_2),\xi(r_3)] = p[\xi(r_1)|\xi(r_2)]. \tag{3.5}$$

The Markov property can be investigated qualitatively by comparison of the empirical distributions of the left and right hand sides of (3.5). As an example, Fig. 3.1(a) shows the two conditional distributions corresponding to the left and right hand sides of (3.5) for left-bounded velocity increments with $\Delta r = \lambda$ (where $\Delta r = r_3 - r_2 = r_2 - r_1$) for the cryogenic free jet at R_λ = 352. The contour plots of the two distributions are almost identical, indicating that the underlying process has the Markov property. A cut through the contour plot for a fixed value of $\xi_2 \equiv \xi(r_2)$ shown in Fig. 3.1(b) confirms that the differences between the two distributions are in fact very small.

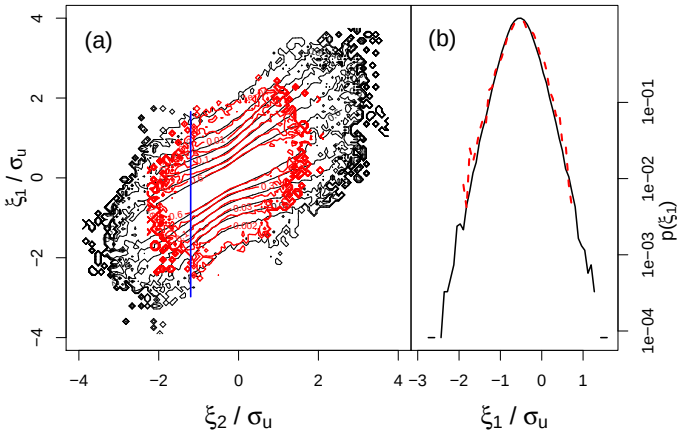

Figure 3.1: (a) Contour plot of the conditional PDFs of the velocity increments, $p(\xi_1|\xi_2)$ (solid), and $p(\xi_1|\xi_2,\xi_3)$ (dashed), where $\xi_i \equiv \xi(r_i)$, with $r_1 = \lambda$, $r_2 = 2\lambda$, $r_3 = 3\lambda$, and $\xi_3 = 0 \pm \sigma_{\xi_3}/8$. (b) The same PDFs at a fixed value of $\xi_2 = -1.2\sigma_u$, which corresponds to a cut through the contour plots in (a) along the vertical straight line. Cryogenic free-jet at $R_\lambda = 352$.

In order to quantify the differences of the distributions, we perform the (Mann-Whitney-)Wilcoxon test [25, 26, 4], described in detail in Appendix 3.5. The Wilcoxon test is a parameter-free statistical procedure to test the hypothesis that two samples of different size originate from the same probability distribution. Since the amount of data points complying with the two conditions on the left hand side of (3.5)

is smaller than the set satisfying the single condition of the right hand side of (3.5) only, the two samples to be compared are necessarily of different size. Therefore the Wilcoxon test is appropriate here. The present implementation of the test computes a statistical test value W which has an expectation of 1 if the hypothesis of the Markov property holds.

In the following analysis, all length scales will be given in units of the Taylor microscale λ, which is estimated from the relation for isotropic turbulence,

$$\frac{\left\langle (u-\langle u\rangle)^2 \right\rangle}{\lambda^2} = \left\langle \left(\frac{\partial u}{\partial x}\right)^2 \right\rangle, \tag{3.6}$$

where $\langle(\partial u/\partial x)^2\rangle$ is calculated by taking the limit of $\lim_{r\to 0}\langle\xi(r)^2\rangle/r^2$ with a linear fit.

Fig. 3.2 shows the results of the Wilcoxon test for the cryogenic helium jet at R_λ = 124 for different parameters q for the condition $\xi_3 = 0 \pm \sigma_{\xi_3}/8$, which is a short notation for $-\sigma_{\xi_3}/8 \le \xi(r_3) \le \sigma_{\xi_3}/8$, with $\sigma_{\xi_3} = \sqrt{\langle\xi(r_3)^2\rangle}$ [2]. For all values of q, we observe an approximately exponential decrease (and subsequent convergence to 1) of W with increasing values of $\Delta r \equiv r_i - r_{i-1}$. We determine a quantity Δr^*, which is defined as the value of Δr where a linear fit to the logarithms of W at small Δr crosses the line of $W = 1$. We then identify this Δr^* with the smallest step size for which the stochastic process in scale has the Markov property. For left-bounded increments, this procedure has been used as a standard method to determine the Einstein-Markov coherence length, defining $l_{EM} = \Delta r^*$ [4, 5, 1] [3]. Fig. 3.3 shows the estimate Δr^* as a function of q.

Figures 3.2 and 3.3 show that Δr^* strongly depends on the nesting parameter q. Fig. 3.4 illustrates that the distances between the left start-points, δr_l, and between the right end-points, δr_r, of two nested increments are in general not identical, except for $q = 1/2$. From our results presented in Fig. 3.3 we now propose *not* to take $\Delta r \equiv \delta r_l + \delta r_r$

[2] We choose this particular data set for a detailed study of the influence of q because it is the one with the best resolution with respect to the Taylor microscale, which is equivalent to approximately 25 sampling steps.

[3] This method might lead to a slight underestimation of l_{EM} because the test values W decrease somewhat slower when they are close to one, but it allows a consistent estimation of l_{EM}, which is important for the comparison of our results.

as measure of step size of the interscale process. Instead the quantity $\delta r \equiv \sup\{\delta r_l, \delta r_r\} = (\frac{1}{2} + |q - \frac{1}{2}|)\Delta r$, which is the larger of the two distances δr_l and δr_r, seems to be more suitable. As shown in Fig. 3.3, $\delta r^* \equiv (\frac{1}{2} + |q - \frac{1}{2}|)\Delta r^*$ is approximately constant in q.

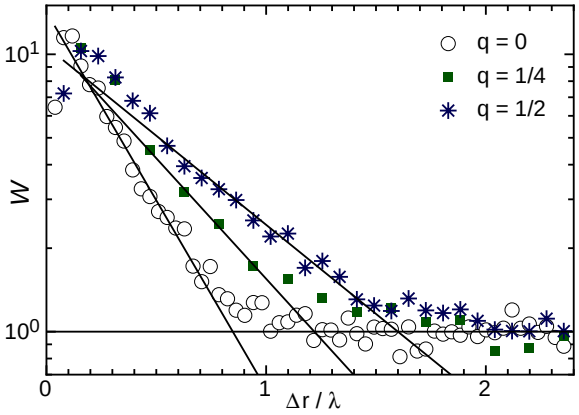

Figure 3.2: Wilcoxon tests for the cryogenic helium jet at R_λ = 124 for different values of q in Eq. (3.1), for $r_1 = \lambda$ in Eq. (3.7) and $\xi_3 = 0 \pm \sigma_{\xi_3}/8$. Lines represent linear fits to the logarithms of W.

The definition of an Einstein-Markov length for nesting parameters q other than 0, 1/2, and 1 is problematical, since for such values, the distances δr_l and δr_r are both non-zero and non-equal, so that there is no consistent single measure of the distance between scales for the corresponding processes.[4] Thus we consider only processes with nesting parameter $q = 0$, 1/2, and 1 for further analysis. In the following, we estimate the Einstein-Markov length by defining $l_{EM} = \delta r^*$, rather than $l_{EM} = \Delta r^*$.

[4] In fact, one could also argue that in these cases it should not be the *longer* of the two distances, $\sup\{\delta r_l, \delta r_r\}$, that matters for Markov properties, but the *shorter* distance, $\inf\{\delta r_l, \delta r_r\}$, which might still cause non-Markovian behavior even when $\sup\{\delta r_l, \delta r_r\}$ is already greater than the Einstein-Markov length. The Wilcoxon test statistics, however, are clearly dominated by the exponential decrease which takes place when the larger distance, $\delta r \equiv \sup\{\delta r_l, \delta r_r\}$, approaches the Einstein-Markov length. A second exponential decrease related to the smaller distance $\inf\{\delta r_l, \delta r_r\}$ is either not present or can not be distinguished from the scattering of W.

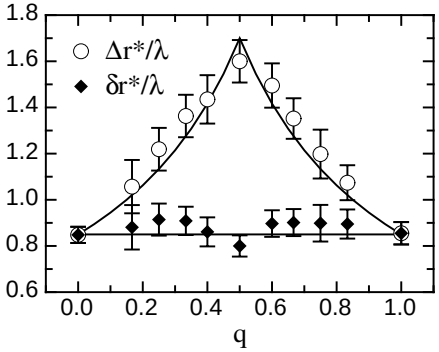

Figure 3.3: Estimated lengths Δr^* and $\delta r^* \equiv (\frac{1}{2} + |q - \frac{1}{2}|)\Delta r^*$ in untis of λ as functions of q for the same data as in Fig. 3.2. The solid lines show an exemplary constant value of $\delta r = 0.85\lambda$ and the corresponding values of $\Delta r = \delta r/(\frac{1}{2} + |q - \frac{1}{2}|)$.

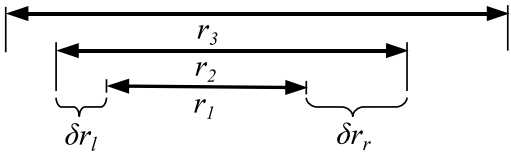

Figure 3.4: Illustration of nested increments for $q = 1/3$ in (3.1).

In Table 3.1, we compare the estimates of the Einstein-Markov coherence length for different flows. The Einstein-Markov lengths based on left-bounded and centered increments are denoted l^l_{EM} and l^c_{EM}, respectively. It was shown in [4] that the length of the base-increment r_1 in (3.5) has very little influence on the estimate of the Einstein-Markov length; in Table 3.1, we chose $r_1 = \lambda$. In accordance with [1], we observe Einstein-Markov lengths for left-bounded increments in the order of $l^l_{EM} \approx (0.8 \pm 0.2)\lambda$. For the cryogenic helium jet and the cylinder wake data, we note a weak decrease of the ratio l^l_{EM}/λ for increasing Reynolds number, which might call for an additional correcting term on the results of [1]. The deeper meaning of this observation deserves further research which goes beyond the scope of the present paper.

flow type	R_λ	l^l_{EM}/λ	l^c_{EM}/λ	$l_{u(x)}/\lambda$
free jet	190	0.73 ± 0.12	0.67 ± 0.10	0.70 ± 0.08
cryogenic	124	0.90 ± 0.09	0.85 ± 0.09	0.87 ± 0.09
free jet	352	0.62 ± 0.09	0.55 ± 0.11	0.66 ± 0.06
cylinder	163	0.80 ± 0.05	0.82 ± 0.10	0.77 ± 0.04
wake	338	0.62 ± 0.05	0.58 ± 0.09	0.53 ± 0.05
fractal	145	0.70 ± 0.06	0.65 ± 0.09	0.87 ± 0.07
square grid	640	0.85 ± 0.15	0.69 ± 0.20	0.79 ± 0.10

Table 3.1: Estimated Einstein-Markov coherence lengths for the process of ξ as a function of scale r based on left-bounded velocity increments, l^l_{EM}, and based on centered increments, l^c_{EM}, in units of the Taylor microscale λ. The quantity $l_{u(x)}$ is the characteristic length scale determined from the exponential decay of the Wilcoxon test value W for the stochastic process of the velocity u as a function of x.

A note on the error estimates. The ratios of l_{EM}/λ in Table 3.1 are based on the estimates of l_{EM} and λ with the methods described above (i.e. a linear fit to $\ln[W_{r_1=\lambda}(\delta r)]$, and a linear extrapolation based on (3.6), respectively). The errors given in Table 3.1 take into account two different error sources for l_{EM}, and one error source for $l_{u(x)}$ and λ. All types of errors are roughly of the same order of magnitude.

The first type of error of the estimate of l^l_{EM}, l^c_{EM}, and $l_{u(x)}$ is the intrinsic error of the fit procedure, denoted σ_{fit}. These intrinsic errors σ_{fit} are the horizontal standard deviations from the linear fits shown exemplarily in Fig. 3.2, i.e. the standard deviations of the values of $\delta r/\lambda$ for the corresponding values of W. Only the values in the range of δr which was used for the fit are considered for the error estimates, of course. The second type of error is due to the choice of a specific method to determine l_{EM}, denoted σ_{method}. For the estimation of σ_{method}, we determine l_{EM} by four different methods and take the standard deviation of the four results as the error. The first method is the one described above, namely a linear fit to the values of W. The second method uses a threshold of $W \leq 1.1$, meaning that we take the first value of δr where $W(\delta r) \leq 1.1$ as the estimate of l_{EM}. The third and fourth methods are the same as the first and second, only that we take $r_1 = L/2$ instead of $r_1 = \lambda$ in the Wilcoxon test. The error for l_{EM} is then given by $\sigma_{\text{l}} = (\sigma^2_{\text{fit}} + \sigma^2_{\text{method}})^{1/2}$. The error of $l_{u(x)}$ is given by $\sigma_{\text{l}} = \sigma_{\text{fit}}$, since in this case we do not use different estimation methods.

The error of the Taylor microscale, σ_λ, is the standard deviation based on two different methods to determine λ. In the first method, the term $\langle(\partial u/\partial x)^2\rangle$ in (3.6) is calculated by taking the limit of $\lim_{r\to 0}\langle\xi(r)^2\rangle/r^2$ with a linear fit. In the second method, the same term is estimated from the relation $\langle(\partial u/\partial x)^2\rangle = \int k^2 E(k) dk$, where $E(k)$ is the power spectrum of the streamwise velocity fluctuations in the streamwise direction [22].

The total error given in Table 3.1 behind the $\pm$ signs of the respective values of l^l_{EM}/λ, l^c_{EM}/λ, and $l_{u(x)}/\lambda$ is given by $\sigma_{\text{total}} = (\sigma^2_{\text{l}} + \sigma^2_\lambda)^{1/2}$.

flow type	R_λ	$\overline{W}_l$	$\overline{W}_c$	$\overline{W}_{u(x)}$
free jet	190	1.00 ± 0.09	0.97 ± 0.08	1.30 ± 0.10
cryogenic	124	1.00 ± 0.09	1.00 ± 0.10	1.10 ± 0.14
free jet	352	0.96 ± 0.10	1.02 ± 0.08	1.23 ± 0.11
cylinder	163	1.01 ± 0.08	0.99 ± 0.11	1.24 ± 0.12
wake	338	1.04 ± 0.10	1.03 ± 0.08	1.19 ± 0.12
fractal	145	0.95 ± 0.10	0.95 ± 0.08	1.32 ± 0.10
square grid	640	0.96 ± 0.12	1.00 ± 0.12	1.20 ± 0.09

Table 3.2: Convergence of the Wilcoxon tests for Markov properties. $\overline{W}_l$ and $\overline{W}_c$ are the averages of the test values W for $\lambda \leq \delta r \leq 2\lambda$ for the left-bounded and centered increments, respectively. The standard deviations of the averages are given after the $\pm$ signs. The length of the base-increment r_1 in eq. (3.5) is the Taylor length, $r_1 = \lambda$. $\overline{W}_{u(x)}$ is the average of W for $\lambda \leq r \leq 2\lambda$ for the process of $u(x)$.

As a central result of this section, we obtain a ratio of $l^c_{EM}/l^l_{EM} = 0.92 \pm 0.06$ for the examined flows. This means that the Einstein-Markov coherence length is only slightly smaller for centered than for left-bounded increments, when the quantity $\delta r \equiv \sup\{\delta r_l, \delta r_r\}$ instead of $\Delta r \equiv r_i - r_{i-1}$ is taken as the effective step size of the interscale process. We take this result as $l^l_{EM} \approx l^c_{EM}$.

The analysis of Markov properties and, hence, the Einstein-Markov length cannot rely on the estimation of the interception point by a fit procedure only. Moreover the convergence of the Wilcoxon test statistics to 1, of course, needs to be verified. Since the Wilcoxon test is a statistical test which naturally contains some scattering, we discuss the statistics of all test values W in the range of $\lambda \leq \delta r \leq 2\lambda$ in order to decide whether the test value converges to 1 or not. The averages and standard deviations of W in the range of $\lambda \leq \delta r \leq 2\lambda$ are presented in Table 3.2. $\overline{W}_l$ and $\overline{W}_c$ denote the average values of W for the interscale processes of $\xi(r)$ for left-bounded and for centered velocity increments, respectively. $\overline{W}_{u(x)}$ denotes the average of W for the process of $u(x)$ (see Section 3.2.3).

In Table 3.2, all values of $\overline{W}_l$ and $\overline{W}_c$ deviate less than one standard deviation from 1 and, hence, show a good convergence indicating the

flow type	R_λ	$\overline{W}_l[r_1 = L/2]$	$\overline{W}_c[r_1 = L/2]$
free jet	190	1.22 ± 0.14	0.97 ± 0.08
cryogenic	124	1.06 ± 0.13	1.00 ± 0.10
free jet	352	1.16 ± 0.14	1.02 ± 0.08
cylinder	163	1.23 ± 0.20	1.03 ± 0.08
wake	338	1.19 ± 0.11	0.99 ± 0.11
fractal	145	0.99 ± 0.11	0.95 ± 0.08
square grid	640	0.92 ± 0.05	1.00 ± 0.12

Table 3.3: As Table 3.2, but for $r_1 = L/2$.

Markov property. However, if instead of $r_1 = \lambda$ we choose a larger scale of the base-increment, $r_1 = L/2$, where L is the integral length scale, the average $\overline{W}_l$ for left-bounded increments deviates between one and two standard deviations from 1 for five out of seven data sets (Table 3.3). This means that although the choice of the base-increment length r_1 does not affect the *estimate* of the Einstein-Markov length [4], it does affect the *quality* (or statistical significance) of the Markov property in the case of left-bounded increments.

This observation can be understood when we compare it to the results by Wächter *et al.* [23], who find that the stochastic process of the increments of uncorrelated Gaussian white noise as a function of scale has the Markov property for centered increments, but not for left-bounded increments. In the case of turbulence, the velocity values at the points x and $x + r_1$ become increasingly uncorrelated with increasing distance r_1. Consequently the results obtained for larger values of r_1 are similar to those for Gaussian white noise in [23].

3.2.3 Markov property of $u(x)$

In the previous section we already noted that the correlations of the velocities at x and $x+r$ decrease with increasing r. This fact could imply that the *velocity* $u(x)$ actually has the Markov property under certain circumstances. Therefore, in this section we examine the velocities $u(x)$ with respect to their Markov property by investigating the validity of the equation

$$p[u(x_1)|u(x_2), u(x_3)] = p[u(x_1)|u(x_2)] \tag{3.7}$$

for different spatial increments $r = x_3 - x_2 = x_2 - x_1$.

We apply the Wilcoxon test as described above to test the distributional validity of (3.7). As for the increments studied in section **??** the test statistic W exhibits an exponential decay at low r (Fig. 3.5). In analogy to the Einstein-Markov length of the interscale process, we can define a characteristic length scale $l_{u(x)}$ for the process of $u(x)$ as the intersection point of the fit with 1. Table 3.1 in the rightmost column contains the resulting fractions $l_{u(x)}/\lambda$. The results are very similar to those of the interscale process: $l_{u(x)}/l^l_{EM} = 1.00 \pm 0.12$. At low r there, hence, seem to be strong similarities between the processes $\xi(r)$ and $u(x)$, and for the latter process, a characteristic length scale $l_{u(x)}$ can be identified which is practically identical to the Einstein-Markov length of the interscale process.

However, Fig. 3.5 shows that the test values W for the process of $u(x)$ do not converge to 1 after the exponential decay. The averages of the Wilcoxon-test values in the range $\lambda \leq r \leq 2\lambda$, $\overline{W}_{u(x)}$, are listed in Table 3.2. These average values deviate from 1 by at least two standard deviations in five out of seven cases, and by more than one standard deviation in six out of seven cases. Thus, for the process of $u(x)$, the hypothesis of the Markov property must be rejected in most cases, and the characteristic length scale $l_{u(x)}$ can not be regarded as an Einstein-Markov length for $u(x)$ in the sense of the word defined in Section 3.1.

The deviations from Markovian behavior of the process of $u(x)$ can also be observed in a graphical comparison of the conditional probability densities of the velocities. Fig. 3.6(a) shows the distributions corresponding to the right and left hand sides of (3.7) for a distance $r = \lambda$. Although the two distributions are quite similar, there are some differences especially for negative values of u_2, which become apparent in Fig. 3.6(b). The errors shown for the distribution $p(u_1|u_2,u_3)$ in this graph indicate that the deviations are significant.[5]

[5]The errors are calculated in the following way: the original data is divided into ten subsets of equal length. Then the conditional probability densities are estimated for all ten subsets, and the variance of the ten results, divided by $\sqrt{10}$, is taken as the error at each point. We should note that the comparison of PDFs on the basis of such error estimates is inferior to statistical tests like the Wilcoxon test.

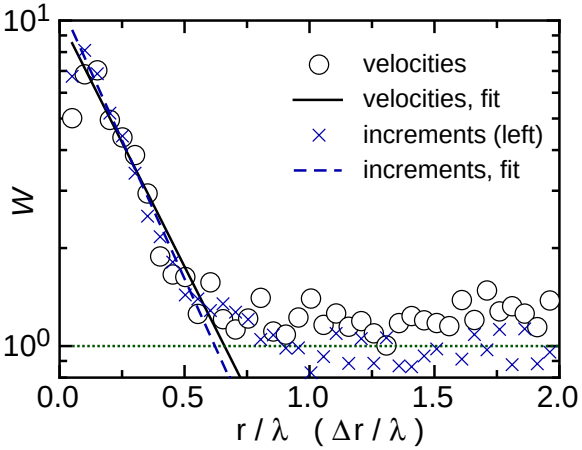

Figure 3.5: Wilcoxon test values $W(r)$ for the cryogenic free-jet at $R_\lambda = 352$ for the process of $u(x)$, based on Eq. (3.7), for $u(x_3) = 0 \pm \sigma_u/8$. For comparison, the test values $W(\Delta r)$ for the interscale process of left-bounded increments are shown for $\xi(r_3) = 0 \pm \sigma_\xi/8$ and $r_1 = \lambda$. The solid and dashed lines represent linear fits to the logarithms of W used to determine $l_{u(x)}$ and l^l_{EM}, respectively.

3.3 Synthetic generation of velocity data with a Markov chain model

In the previous section, we saw that the Wilcoxon test value W for the process of $u(x)$ shows the same exponential decay at small step sizes as for the stochastic process of the velocity increments $\xi(r)$, and that a characteristic length scale $l_{u(x)} \approx l_{EM}$ can be estimated from this exponential decay. Since the Wilcoxon test for $u(x)$ does not relax to 1, however, this process does not have the Markov property. We now want to investigate which main statistical properties of turbulence can be reproduced based on the *assumption* of the Markov property for the process of $u(x)$. In other words, we want to know for which features of turbulence the deviations from Markovian behavior observed in Figures 3.5 and 3.6, and in Table 3.2, are important.

In order to address the impact of the deviations from the Markov

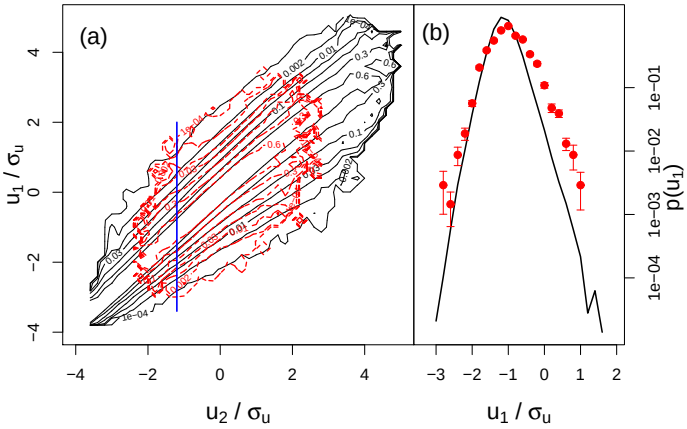

Figure 3.6: (a) Contour plot of the conditional PDFs of the velocities, $p(u_1|u_2)$ (solid), and $p(u_1|u_2,u_3)$ (dashed), where $u_i \equiv u(x_i)$, for $x_2 = x_1 - \lambda$, $x_3 = x_1 - 2\lambda$, and $u_3 = 0 \pm \sigma_u/8$. (The mean flow velocity $\overline{u}$ has been subtracted from the velocity, i.e. in this graph, u denotes the velocity *fluctuation*). (b) The same PDFs at a fixed value of $u_2 = -1.2\sigma_u$, which corresponds to a cut through the contour plots in (a) along the vertical straight line. Cryogenic free-jet at $R_\lambda = 352$.

property, we apply the following procedure: We calculate the matrix of transition probabilities from one velocity value u at the position x to the next value at the position $x+r$, and then generate synthetic data from this empirical transition matrix. This non-parametric method is entirely based on the experimental data and makes no other assumption than that of the Markov property. It has been applied to atmospheric wind speed data, for example in [27, 28]. As step size r of the process we choose the Taylor microscale λ, which is about the Einstein-Markov coherence length. The original data series $u(x)$ is transformed into a series of discrete values u_i^* with a limited number of possible values. For example, the number of different velocity values is reduced from 1770 to N = 118 in the case of the air free jet data, and from 2^{15} to N = 128 in the case of the cryogenic free jet data. From this data series, we obtain an $N \times N$-matrix of the conditional transition probabilities $P(u_i^*|u_{i-1}^*)$, which are equivalent to the probabilities $p[u(x)|u(x-r)]du$, where du is

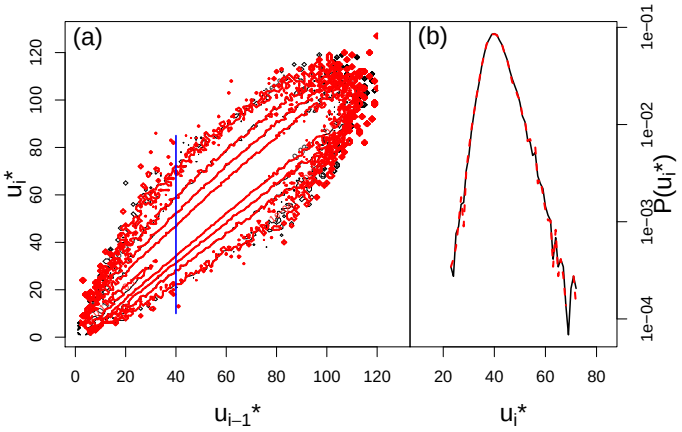

Figure 3.7: (a) Contour plots of the transition matrices, $P(u_i^*|u_{i-1}^*)$, of the original data (solid), and of the reconstructed data (dashed). (b) $P(u_i^*|u_{i-1}^*)$ for the same data at a fixed value of u_{i-1}^*, which corresponds to a cut through the contour plots in (a) along the vertical line. Cryogenic free jet at $R_\lambda = 352$.

the bin size. In the next step, a synthetic data series of discrete velocity values is generated, using the empirical transition matrix. The generated data have the same length as the original measured data. We check the correct implementation of this procedure by calculating the transition matrix of the synthetic data and plotting it into the same graph with the transition matrix of the original data. This has been done in figure 3.7 for the cryogenic helium jet at $R_\lambda = 352$.

If the generated synthetic data set is sufficiently long, the Markov chain model, by construction, reproduces correctly the following statistical properties of the original data: the distribution of the velocity, $p(u)$; the distribution of the velocity increment at the smallest scale, $p[\xi(\lambda)]$; and the conditional distribution of the velocity for the elementary step size λ, $p[u(x)|u(x-\lambda)]$, which is equivalent to the transition matrix itself.

In order to see differences between the original and reconstructed data, we have to look at the two- and three-point statistics at scales larger than λ. Fig. 3.8 shows the distributions of the velocity increment

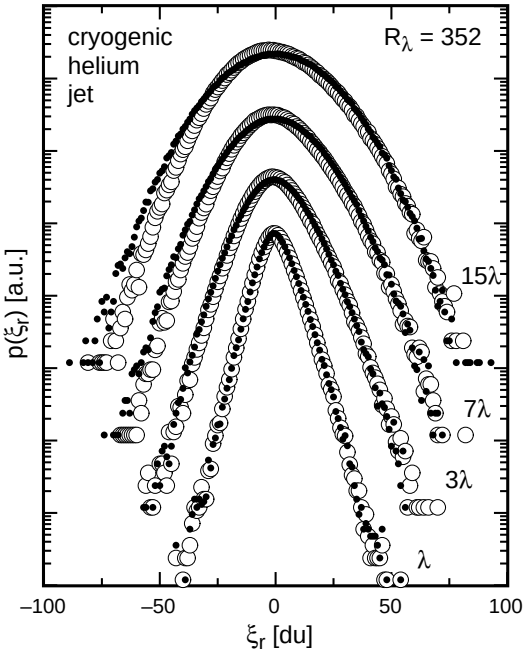

Figure 3.8: Probability densities of the velocity increments, $p(\xi_r)$, where ξ_r is given in units of the bin size du of the transition matrix. From bottom to top, the increment scales are $r = \lambda$, 3λ, 7λ, and $15\lambda \approx L$, where L is the integral length. Open circles represent the distributions of the original data, dots those of the data reconstructed with the empirical transition matrix. The plots are shifted vertically for convenience. Cryogenic free jet at R_λ = 352.

$\xi_r \equiv \xi(r)$ at different scales r. The shapes of the increment distributions of the original and reconstructed data do not seem to be very different at first glance. Also the conditional distributions $p(\xi_1|\xi_2)$ at large scales shown in Fig. 3.9 do agree remarkably well.

Since the visual comparison of increment distributions might not be sufficient, we look at the moments (structure functions) and related quantities of these distributions. Fig. 3.10 shows the structure functions $S_n(r) \equiv \langle \xi(r)^n \rangle$ of orders $n = 2, 3, 4$ of three of the data sets. There

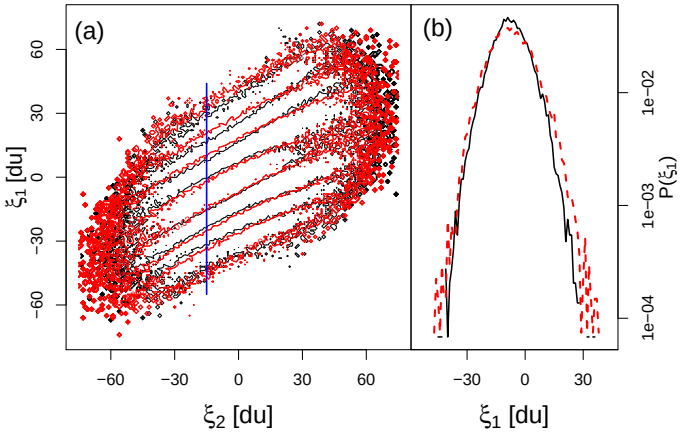

Figure 3.9: (a) Contour plots of the conditional probabilities of the velocity increments, $P[\xi_1(r_1 = 7\lambda)|\xi_2(r_2 = 14\lambda)]$, for the same original (solid) and reconstructed (dashed) data as in fig. 3.8, in units of du. (b) Cut through the contour plots in (a) along the vertical straight line, which corresponds to a fixed value of ξ_2.

are significant differences between the structure functions of the original and reconstructed data, especially in the case of $n = 3$. While for the original data $S_3(r)$ is approximately linear in r in the inertial range, $\lambda < r < L$, in agreement with Kolmogorov's four-fifths law for homogeneous isotropic turbulence [29, 30], it tends to zero after a short increase for the reconstructed data.

Fig. 3.11 shows the power spectra of three data sets, which are related to the second order structure functions $S_2(r)$. The spectra of the original and reconstructed data agree quite well. They are even practically identical for the fractal grid turbulence, which is characterized by a low ratio of the integral length to the Taylor microscale even at high Reynolds numbers, and which displays less intermittency than other types of turbulence [22].

Fig. 3.12 shows that the flatness of the increment distributions, $F(r) = \langle \xi(r)^4 \rangle / \langle \xi(r)^2 \rangle^2$, which is a measure of intermittency, decreases much faster for the reconstructed than for the original data. This also applies to the fractal grid data, where the differences between orig-

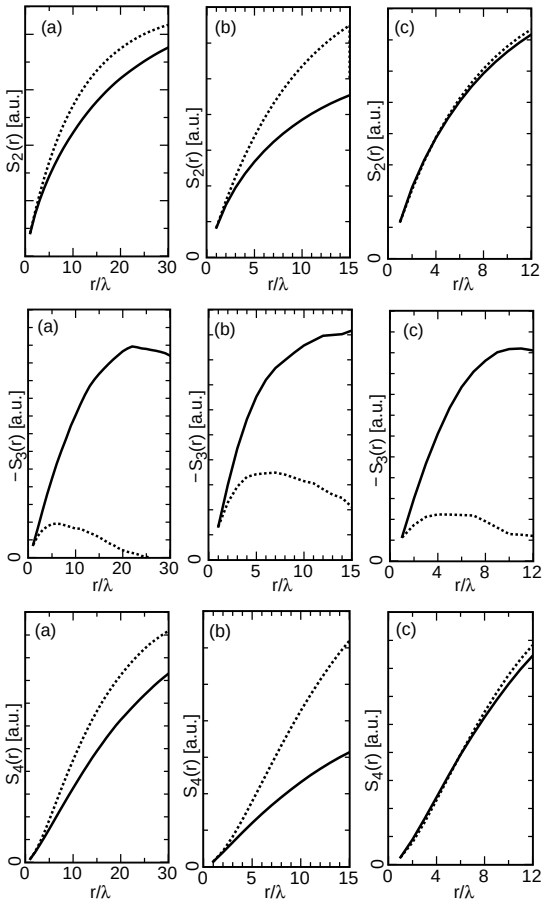

Figure 3.10: Structure functions $S_n(r) = \langle \xi(r)^n \rangle$ for $n = 2, 3, 4$ (from top to bottom) of the original (solid curve) and reconstructed data (dotted curve). (a) cryogenic helium jet at R_λ = 352, (b) cylinder wake at R_λ = 338, (c) fractal square grid at R_λ = 640.

inal and reconstructed second and fourth order structure functions in Fig. 3.10 do not appear to be significant at first glance.

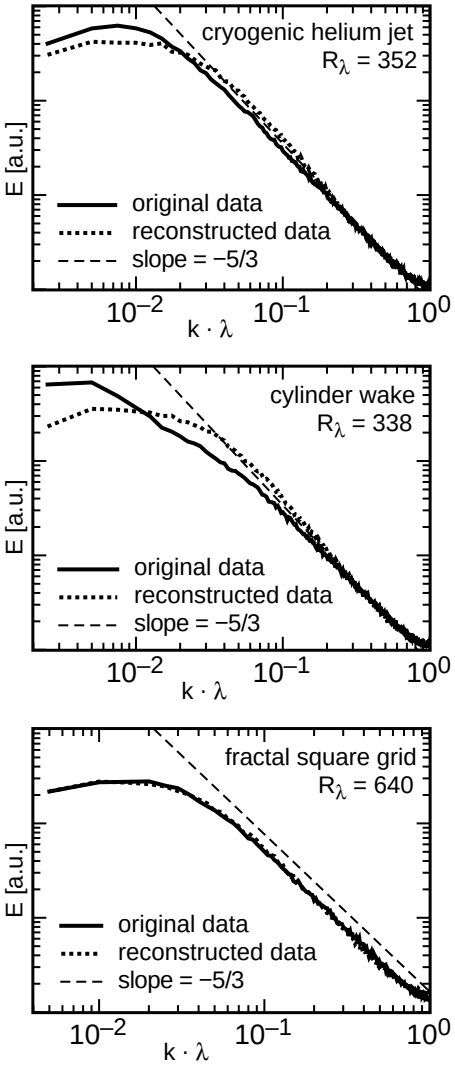

Figure 3.11: Power spectra of the original and reconstructed data for the cryogenic helium jet at R_λ = 352, the cylinder wake at R_λ = 338, and the fractal square grid at R_λ = 640.

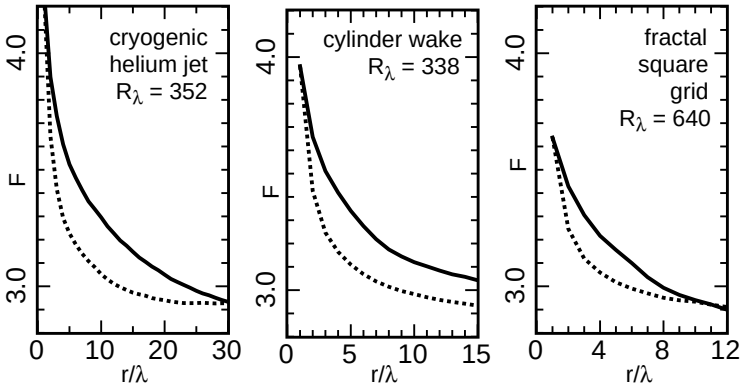

Figure 3.12: Flatness $F(r) = \langle \xi(r)^4 \rangle / \langle \xi(r)^2 \rangle^2$ of the velocity increments of the original (solid) and reconstructed (dotted) data for the cryogenic free jet at R_λ = 352, the cylinder wake at R_λ = 338, and the fractal square grid at R_λ = 640.

3.4 Conclusions

We investigated the Markov property of the velocity increments ξ *in scale* r for different nesting structures of the increments. In the past, there have been uncertainties concerning the impact of the nesting structure on the Markov property, which could be resolved with the present contribution. If a reasonable definition of the effective step size of the stochastic process is applied, the Einstein-Markov coherence length l_{EM} for all nesting structures is of the order of magnitude of the Taylor microscale.

A possible interpretation of the existence of an Einstein-Markov coherence length in turbulence is that there might be small-scale coherent structures which 'smooth out' the stochastic character of the velocity field, and which might be associated with viscosity [1]. This interpretation of the Einstein-Markov coherence length would be consistent with the result of Yakhot [31] that the largest 'dissipation scale' in turbulence scales with $Re^{-1/2}$, like the Taylor microscale.

For the stochastic process of the velocity $u(x)$, we analogously estimate a characteristic length scale $l_{u(x)}$ from a statistical test for

the Markov property, and find that this characteristic scale is equivalent to the Einstein-Markov coherence length of the interscale process: $l_{u(x)} \approx l_{EM}$. This fact, once again, emphasizes the physical relevance of the Einstein-Markov length of a data set. In the case of $u(x)$, however, the convergence to the Markov property is not perfect. Nevertheless, some important statistical properties of experimental turbulence data, like power spectra and conditional increment distributions, can be reconstructed remarkably well by a simple Markov chain model based on a matrix of transition probabilities, proposed in [27]. For practical purposes of generating synthetic turbulence-like data, the Markov chain model is much more successful for stationary turbulence data than it was found for atmospheric wind speed data, where great differences between the power spectra of original and synthetic data have been observed [28]. Two fundamental properties of homogeneous isotropic turbulence, namely inertial-range intermittency and Kolmogorov's four-fifths law, however, can not be reproduced correctly with the Markov chain model, which is a one-scale model.

Thus, we conclude that a complete statistical description of the turbulent velocity must be a multi-scale description. Such a description is given by the stochastic differential equations of the interscale process [2, 3, 4, 5, 8].

We thank C. Renner, O. Chanal, and B. Chabaud for the free jet data, S. Lück for the cylinder wake data, and R. Seoud and C. Vassilicos for the fractal grid data. We also thank C. Vassilicos for interesting discussions on the subject. R. S. and J. P. acknowledge financial support by DFG Grant No. PE 478/14-1.

3.5 Appendix: The (Mann-Whitney-)Wilcoxon test

The null hypothesis to be tested by the Wilcoxon test [25, 26, 4] is that the probability density functions $p(y)$ and $\tilde{p}(z)$ of the stochastic variables y and z are identical. In the case of (3.5), the two stochastic variables are $y = \xi_1(r_1)|_{\xi_2(r_2)}$, and $z = \xi_1(r_1)|_{\xi_2(r_2),\xi_3(r_3)}$. For (3.7), they are $y = u_1(x_1)|_{u_2(x_2)}$, and $z = u_1(x_1)|_{u_2(x_2),u_3(x_3)}$. Two samples $y_1,...,y_n$ and $z_1,...,z_m$ of independent realizations of the variables are taken from the data. We take values which are separated by one integral length L to be sufficiently independent from each other for the purpose of the test, in order not to reduce the sample sizes too much. Then, the number of values z_j with $y_j < z_i$ is counted for each z_i and summed over i:

$$Q = \sum_{i=1}^{m} \sum_{j=1}^{n} \alpha_{ij}, \quad \alpha_{ij} = \begin{cases} 1 : y_j < z_i \\ 0 : y_j \geq z_i \end{cases} . \tag{3.8}$$

Under the null hypothesis, the quantity Q is Gaussian distributed with mean value $\mu_0(n,m) = nm/2$, and, for $n,m > 25$, standard deviation $\sigma_0(n,m) = \sqrt{nm(n+m+1)/12}$. Then the quantity

$$\Delta Q = \frac{|Q - \mu_0(n,m)|}{\sigma_0(n,m)}, \tag{3.9}$$

which is the absolute value of a standard normal distributed variable, has a mean value of $\sqrt{2/\pi}$. In the present implementation of the test, the quantity

$$\Delta Q^* \equiv \Delta Q / \sqrt{2/\pi} \tag{3.10}$$

is calculated for a fixed value of ξ_3 (respectively u_3) for a number of 100 bins for ξ_2 (u_2), which span the complete range of ξ_2 (u_2). The mean value $W \equiv \langle \Delta Q^* \rangle$ is calculated by taking the average over the 100 values of ΔQ^*. Under the null hypothesis of the Markov property, the expectation value of W is 1.

Bibliography

[1] S. Lück, C. Renner, J. Peinke, and R. Friedrich. The Markov–Einstein cohernce length—a new meaning for the Taylor length in turbulence. *Phys. Lett. A*, 359:335–338, 2006.

[2] R. Friedrich and J. Peinke. Description of a turbulent cascade by a Fokker-Planck equation. *Phys. Rev. Lett.*, 78:863–866, 1997.

[3] R. Friedrich, J. Zeller, and J. Peinke. A note on three-point statistics of velocity increments in turbulence. *Europhys. Lett.*, 41:153–158, 1998.

[4] C. Renner, J. Peinke, and R. Friedrich. Experimental indications for Markov properties of small-scale turbulence. *J. Fluid Mech.*, 433:383–409, 2001.

[5] C. Renner, J. Peinke, R. Friedrich, O. Chanal, and B. Chabaud. Universality of small scale turbulence. *Phys. Rev. Lett.*, 89:124502, 2002.

[6] M. Tutkun and L. Mydlarski. Markovian properties of passive scalar increments in grid-generated turbulence. *New J. Phys.*, 6:49, 2004.

[7] R. Stresing, J. Peinke, R. E. Seoud, and J. C. Vassilicos. Defining a new class of turbulent flows. *Phys. Rev. Lett.*, 104(19):194501, 2010.

[8] R. Stresing and J. Peinke. Towards a stochastic multi-point description of turbulence. *New J. Phys.*, 12:103046, 2010.

[9] M. Wächter, F. Riess, H. Kantz, and J. Peinke. Stochastic analysis of surface roughness. *Europhys. Lett.*, 64:579–585, 2003.

[10] G. R. Jafari, S. M. Fazeli, F. Ghasemi, S. V. Allaei, M. R. R. Tabar, A. I. Zad, and G. Kavei. Stochastic analysis and regeneration of rough surfaces. *Phys. Rev. Lett.*, 91:226101, 2003.

[11] P. Manshour, S. Saberi, M. Sahimi, J. Peinke, A. F. Pacheco, and M. R. R. Tabar. Turbulencelike behavior of seismic time series. *Phys. Rev. Lett.*, 102:014101, 2009.

[12] C. Renner, J. Peinke, and R. Friedrich. Evidence of Markov properties of high frequency exchange rate data. *Physica A*, 298:499–520, 2001.

[13] M. Ausloos and K. Ivanova. Dynamical model and nonextensive statistical mechanics of a market index on large time windows. *Phys. Rev. E*, 68, 2003.

[14] A. P. Nawroth and J. Peinke. Medium and small scale analysis of financial data. *Physica A*, 382:193, 2007.

[15] A. Einstein. Über die von der molekularkinetischen Theorie der Wärme geforderte Bewegung von in ruhenden Flüssigkeiten suspendierten Teilchen. *Ann. d. Phys.*, 322(8):549–560, 1905.

[16] M. R. R. Tabar, M. Sahimi, and F. Ghasemi et al. *Modelling critical and catastrophic phenomena in geoscience*, volume 705 of *Lecture Notes in Physics*, pages 281–301. Springer, 2006.

[17] M. J. Fisher and P. O. Davies. Correlation measurements in a nonfrozen pattern of turbulence. *J. Fluid. Mech.*, 18.

[18] H. Risken. *The Fokker-Planck Equation*. Springer Verlag, 1996.

[19] A. P. Nawroth, J. Peinke, D. Kleinhans, and R. Friedrich. Improved estimation of Fokker-Planck equations through optimisation. *Phys. Rev. E*, 76:056102, 2007.

[20] O. Chanal, B. Chabaud, B. Castaing, and B. Hébral. Intermittency in a turbulent low temperature gaseous helium jet. *Eur. Phys. J. B*, 17:309–317, 2000.

[21] S. Lück. *Turbulente Nachlaufströmungen*. Der Andere Verlag, Tönning, 2001.

[22] R. E. Seoud and J. C. Vassilicos. Dissipation and decay of fractal-generated turbulence. *Phys. Fluids*, 19:105108, 2007.

[23] M. Wächter, A. Kouzmitchev, and J. Peinke. Increment definitions for scale-dependent analysis of stochastic data. *Phys. Rev. E*, 70:055103, 2004.

[24] D. Kleinhans. *Stochastische Modellierung komplexer Systeme*. PhD thesis, Universität Münster, Münster, Germany, 2008.

[25] F. Wilcoxon. Individual comparisons by ranking methods. *Biometrics Bull.*, 1(6):80–83, 1945.

[26] H. B. Mann and D. R. Whitney. On a test of whether one of two random variables is stochastically larger than the other. *Ann. Math. Stat.*, 18:50–60, 1947.

[27] R. H. Kirchhoff, F. C. Kaminsky, and C. Y. Syu. Synthesis of wind speed using a markov chain. In *Eighth ASME Wind Energy Symposium*, 1989.

[28] F. C. Kaminsky, R. H. Kirchhoff, C. Y. Syu, and J. F. Manwell. A comparison of alternative approaches for the synthetic generation of a wind speed time series. *J. Sol. Energy Eng.*, 113:280–289, 1991.

[29] A. N. Kolmogorov. Dissipation of energy in locally isotropic turbulence. *Dokl. Akad. Nauk SSSR*, 32:16–18, 1941, english version in: *Proc. R. Soc. Lond. A*, 434:15–17, 1991.

[30] U. Frisch. *Turbulence – The legacy of A. N. Kolmogorov*. Cambridge University Press, 1995.

[31] V. Yakhot. Pressure–velocity correlations and scaling exponents in turbulence. *J. Fluid Mech.*, 495:135–143, 2003.

Chapter 4

Stochastic multi-point description of turbulence[1]

Abstract In previous works it was found that the multi-scale statistics of homogeneous isotropic turbulence can be described by a stochastic "cascade" process of the velocity increment from scale to scale, which is governed by a Fokker-Planck equation. We now show how this description can be extended in order to obtain the complete multi-point statistics of the velocity field. We extend the stochastic cascade description by conditioning on the velocity value itself, and find that the corresponding process is also governed by a Fokker-Planck equation, which contains as a leading term a simple additional velocity-dependent coefficient in the drift function. Taking the velocity-dependence of the Fokker-Planck equation into account, the multi-point statistics in the inertial range can be expressed by two-scale statistics of velocity increments, which are equivalent to three-point statistics of the velocity field. Thus, we propose a stochastic three-point closure for the velocity field of homogeneous isotropic turbulence.

[1] Published as R. STRESING and J. PEINKE: Towards a stochastic multi-point description of turbulence, *New J. Phys.* **12**, 103046, 2010.

4.1 Introduction

There has been extensive research activity aimed at achieving a stochastic description of the complexity of turbulent velocity fields. A central focus has been put on the case of homogeneous isotropic turbulence in the hope to simplify this attempt. Over the last decades many works on the statistical properties of velocity increments

$$\xi(r) = U(x+r) - U(x)$$

have been published. Two-point statistics with respect to the increments are given by the probability density function (PDF) $p[\xi(r)]$.[2] The knowledge of $p[\xi(r)]$ is equivalent to the knowledge of all structure functions $S_n(r) = \langle \xi(r)^n \rangle$ (c.f. [1]).

By focussing on the statistics of increments, the actual values of the velocity $U(x)$ are somehow filtered out. However, there is experimental evidence that the velocity increments statistically depend on the velocity itself [2, 3, 4]. In other words, the 'sweeping decorrelation hypothesis', which implies statistical independence of small-scale quantities like velocity increments of the large-scale excitation represented by the velocity itself, is in general not valid for turbulence. Hosokawa [5] takes the quantity $\xi_+(r) := U(x+r) + U(x)$ as a measure of the large-scale dynamics of turbulence. He shows that for homogeneous turbulence, the assumption of statistical independence of the small-scale increment ξ and the large-scale quantity ξ_+ is inconsistent with the existence of a non-vanishing third-order structure function $\langle \xi(r)^3 \rangle \neq 0$. This argument also rules out the sweeping decorrelation hypothesis. Thus, by focussing exclusively on velocity increments, some information about the complexity of turbulence is lost.

In the present paper, we will go beyond these findings of interdependence of velocity increments (i.e. single-scale statistics) and velocities (i.e. single-point statistics), by investigating the relation between multi-scale and multi-point statistics. We are interested in these quantities because they allow a more profound characterization of the velocity field than the increment statistics $p[\xi(r)]$, which include only a single scale.

Over the last decades, different attempts have been made to describe turbulence by scale-dependent stochastic models like, for example, the

[2] Different types of brackets, $(\cdot)$ and $[\cdot]$, are used to facilitate reading.

multifractal model (cf. [1, 6, 7]), which, in modified forms, has also been applied to financial data (cf. [8, 9, 10, 11, 12]). Yakhot [13] presents arguments form dynamic theory which are consistent with the multifractal approach, showing that the PDF of the small-scale velocity fluctuations includes information about the large scale dynamics.

Friedrich and Peinke [14, 15] suggested a different scale-dependent description of turbulence, based on a Fokker-Planck equation for the stochastic process of the velocity increment ξ as a function of scale r. This approach is based on the experimental evidence that the stochastic process of $\xi(r)$ has the Markov property for step sizes Δr larger than the so-called Einstein-Markov coherence length l_{EM}, which is of the order of the Taylor microscale, $l_{EM} \approx \lambda$ [16]. The method gives access to the multi-scale statistics expressed by the joint N-scale PDF $p[\xi(r_1), \xi(r_2), \ldots, \xi(r_N)]$ for N differently chosen scales r_j, which are separated by at least one Einstein-Markov length. The relevant information about the stochastic process, i.e. the coefficients of the Fokker-Planck equation, can be estimated directly from given experimental data (cf. [17, 18, 19, 20, 21, 22]).

Nawroth *et al.* [23] noticed that this multi-scale description can also be used for the generation of synthetic time series with the same statistical multi-scale properties as, for example, a given turbulent velocity time series, or for the prediction of financial time series [24]. They also noticed that it is necessary to take into account the statistics of the velocity itself in order to obtain stationary synthetic data [23]. In the present work, we want to go beyond this approach and show precisely how the joint N-scale PDF $p[\xi(r_1), \xi(r_2), \ldots, \xi(r_N)]$ is related to the joint (N+1)-point PDF $p[U(x), U(x+r_1), \ldots, U(x+r_N)]$. As a consequence of Markov properties of the velocity increments, the multi-point statistics can be obtained based on the knowledge of the velocity field at three points. Thus we propose a stochastic three-point closure for homogeneous isotropic turbulence.

The paper is organized as follows: In Section 4.2, we examine the relation of multi-scale and multi-point statistics. We derive a velocity-dependent Fokker-Planck equation for the velocity increments, which gives access to the multi-point statistics. In Section 4.3, we present experimental evidence for the validity of such a stochastic description, and we examine the empirical velocity dependence of the Fokker-Planck equation. Section 4.4 concludes the paper.

4.2 Multi-scale and multi-point statistics

In the following, we use the notation $u := U - \bar{U}$ for the velocity fluctuation, where $\bar{U}$ is the mean flow velocity. We also use the short-hand notations $u_i := u(x_i)$ and $u_{i+j} := u(x_i + r_j)$, and for the velocity increment ξ at scale r_j we write:

$$\begin{aligned} \xi_j \equiv \xi(r_j) &= U(x_i + r_j) - U(x_i) \\ &= u(x_i + r_j) - u(x_i). \end{aligned} \tag{4.1}$$

The starting point of our work is the finding that the N-scale statistics of velocity increments can be expressed by two-scale conditional probability densities $p(\xi_j|\xi_{j+1})$. More precisely in several papers, cf. [18, 19, 20, 21, 22], it has been shown by experimental evidence that the stochastic process of the velocity increment ξ in scale r has Markov properties, i.e. that

$$p(\xi_j|\xi_{j+1}, \xi_{j+2}, ..., \xi_{j+N}) = p(\xi_j|\xi_{j+1}), \tag{4.2}$$

where the process direction has been chosen from large to small scales, by sorting the scale variables r_j as $r_1 < r_2 < ... < r_N$. This equation is usually studied for $N = 2$, as an adequate simplification for finite data sets [14],

$$p(\xi_j|\xi_{j+1}, \xi_{j+2}) = p(\xi_j|\xi_{j+1}). \tag{4.3}$$

We should note that (4.2) and (4.3) only hold for step sizes $\Delta r := r_{j+1} - r_j$ which are larger than the so-called Einstein-Markov coherence length l_{EM}, which is of the order of magnitude of the Taylor microscale λ [16, 25]. If (4.2) holds, the N-scale joint probability density function of the velocity increments can be expressed by a product of conditional PDFs,

$$p(\xi_1, \ldots, \xi_N) = p(\xi_1|\xi_2)p(\xi_2|\xi_3)\ldots p(\xi_{N-1}|\xi_N)p(\xi_N). \tag{4.4}$$

As a next step we consider the (N+1)-point statistics which can be expressed by

$$\begin{aligned} p(u_i, u_{i+1}, \ldots, u_{i+N}) &= p(\xi_1, \ldots, \xi_N, u_i) \\ &= p(\xi_1, \ldots, \xi_N|u_i) \cdot p(u_i), \end{aligned} \tag{4.5}$$

as can be easily seen, since the increments ξ_j of this equation are calculated from the velocity values which appear at the left-hand side.[3] Let us assume that the Markov property of the interscale process is conserved when the process is conditioned on the velocity, i.e. let us assume that

$$p(\xi_j|\xi_{j+1},\xi_{j+2},...,\xi_N,u_i) = p(\xi_j|\xi_{j+1},u_i), \tag{4.6}$$

which can be simplified to a sufficient condition for finite data,

$$p(\xi_j|\xi_{j+1},\xi_{j+2},u_i) = p(\xi_j|\xi_{j+1},u_i). \tag{4.7}$$

Eq. (4.6) implies the following factorization of the multipoint joint PDF:

$$p(u_i,u_{i+1},\dots,u_{i+N}) = p(\xi_1|\xi_2,u_i)\dots p(\xi_{N-1}|\xi_N,u_i)\,p(\xi_N|u_i)\,p(u_i). \tag{4.8}$$

The evolution of the conditional PDFs of (4.8) in scale r_j can be expressed by a Kramers-Moyal expansion [26],

$$-r_j\frac{\partial}{\partial r_j}p(\xi_j|\xi_k,u_i) = \sum_{q=1}^{\infty}\left(-\frac{\partial}{\partial\xi_j}\right)^q\left[D^{(q)}(\xi_j,r_j,u_i)p(\xi_j|\xi_k,u_i)\right], \tag{4.9}$$

where $r_k > r_j$, with the Kramers-Moyal coefficients

$$\begin{aligned} D^{(q)}(\xi_j,r_j,u_i) &= \lim_{\delta r\to 0}\frac{r_j}{q!\,\delta r}\langle\left[\xi_j'(r_j-\delta r,u_i)-\xi_j(r_j,u_i)\right]^q\rangle \\ &= \lim_{\delta r\to 0}\frac{r_j}{q!\,\delta r}\int_{-\infty}^{\infty}(\xi_j'-\xi_j)^q\,p[\xi_j'(r_j-\delta r,u_i)|\xi_j(r_j,u_i)]d\xi_j'. \end{aligned} \tag{4.10}$$

Note that in contrast to the usual notation, we multiplied both sides of (4.9) by r_j, and we have a negative sign on the left hand side due to the process direction from large to small scales. If the Kramers-Moyal coefficient of fourth order, $D^{(4)}$, vanishes, the expansion truncates after

[3] We should note that equations like $p(u_i,\dots) = p(\xi_1,\dots)$ should actually be written as $p(u_i,\dots) = \tilde{p}(\xi_1,\dots)$. But since the notation would get quite complicated if we denoted each different PDF by a different symbol, we use a simplified notation where different arguments of $p(\cdot)$ imply different functions.

the second term and becomes a Fokker-Planck equation [26],

$$-r_j \frac{\partial}{\partial r_j} p(\xi_j|\xi_k,u_i) = -\frac{\partial}{\partial \xi_j}\left[D^{(1)}(\xi_j,r_j,u_i)p(\xi_j|\xi_k,u_i)\right] + \frac{\partial^2}{\partial \xi_j^2}\left[D^{(2)}(\xi_j,r_j,u_i)p(\xi_j|\xi_k,u_i)\right]. \tag{4.11}$$

In the same way, a velocity-independent Fokker-Planck equation can be derived from (4.4),

$$-r_j \frac{\partial}{\partial r_j} p(\xi_j|\xi_k) = -\frac{\partial}{\partial \xi_j}\left[\tilde{D}^{(1)}(\xi_j,r_j)p(\xi_j|\xi_k)\right] + \frac{\partial^2}{\partial \xi_j^2}\left[\tilde{D}^{(2)}(\xi_j,r_j)p(\xi_j|\xi_k)\right]. \tag{4.12}$$

It has been shown for homogeneous isotropic turbulence that the coefficient $\tilde{D}^{(4)}(\xi_j,r_j)$ can in fact be neglected [18, 20]. Therefore, the Fokker-Planck equation (4.12) is an adequate description of the inter-scale process of the velocity increments, giving access to the N-scale joint PDF of (4.4).

In order to step from the description of multi-scale to multi-point statistics, we have to examine the validity of (4.7), check whether or not the coefficient $D^{(4)}(\xi_j,r_j,u_i)$ can be neglected, and study the empirical dependence of the Fokker-Planck equation (4.11) on the velocity u_i. This will be done in the next section.

4.3 Experimental results

We analyze hot-wire measurement data from three different flow types at different Reynolds numbers. The first flow type is the wake of a cylinder with diameter D = 2 cm in a wind tunnel at downstream distance x = 100 D, for Taylor microscale Reynolds numbers R_λ in the range from 86 to 338 [27]. We use the data at R_λ = 338 for the most detailed analysis. This data is characterised by a dissipation scale η = 0.10 mm, Taylor microscale λ = 3.7 mm, and integral scale L = 119 mm. The second flow type is an axisymmetric air free jet at 145 nozzle-diameters distance from the nozzle, at R_λ = 190, with η = 0.25 mm, λ = 6.6 mm, and L = 67 mm. This data is described in detail in [18]. Finally, we

also analyze data from the flow behind a so-called space-filling fractal square grid, described in detail in [28], measured at different positions in the decay region of the turbulence in the wind tunnel, for different flow speeds, at Reynolds numbers R_λ between 175 and 740. The cylinder wake and free jet data sets have a total length of $12.5 \cdot 10^6$ values each, and the fractal grid data sets have a length of $3 \cdot 10^6$ values each. We analyze the streamwise velocity component of the cylinder wake and fractal grid data, which has been measured with cross-wire probes. The free jet data has been measured with a single wire.

We examine the dependence of the conditional PDFs of the velocity increments on the velocity itself by comparing both sides of the equation

$$p(\xi_1|\xi_2, u_i) = p(\xi_1|\xi_2). \tag{4.13}$$

Note that if (4.13) would hold, the Fokker-Planck equations (4.11) and (4.12) would be identical. In Fig. 4.1, we compare the contour plots of both conditional distributions of (4.13) for the free jet at scales $r_1 = 2\lambda \approx L/4$ and $r_2 = 2r_1$ for two different values of u_i. The distributions agree almost perfectly for $u_i = 0$, while for a larger velocity, $u_i = 2\sigma_u$ (where $\sigma_u = \sqrt{\langle u^2 \rangle}$), the distribution $p(\xi_1|\xi_2, u_i)$ is slightly shifted downward with respect to the other distribution $p(\xi_1|\xi_2)$. According to the errors of $p(\xi_1|\xi_2, u_i)$ shown in this figure, the shift is statistically significant.[4] Such a shift of the conditional PDF for velocities $u_i \neq 0$ can be observed at any scale r_1 for all examined flows. As we will see below, this shift will lead to a velocity-dependent term in the drift function of the Fokker-Planck equation.

In Section 4.2, we argued that the multi-point statistics might be obtained from the velocity-dependent Fokker-Planck equation (4.11) of the interscale process. A necessary condition for this description to hold is the validity of (4.7), which states that the Markov property of the interscale process is conserved under the additional condition of u_i. In order to verify the validity of (4.7), we apply the (Mann-Whitney-)Wilcoxon test [29, 30, 18], which tests whether or not two samples

[4] The errors shown in Fig. 4.1 are calculated in the following way: the original data is divided into ten subsets of equal length, the conditional probability densities are estimated for all ten subsets, and the variance of the ten results, divided by $\sqrt{10}$, is taken as the error at each point. We should note that such error estimates can only serve as a rough estimate of the statistical significance of the shift of the PDFs. With the Wilcoxon-test, described in Section 4.5, it can be shown that (4.13) is only valid as an approximation for very small scales $l_{EM} < r_1 \ll L$, and not for very large values of $|u_i| \approx 2\sigma_u$. To save space, these results are not presented here [see Section 5.4.2].

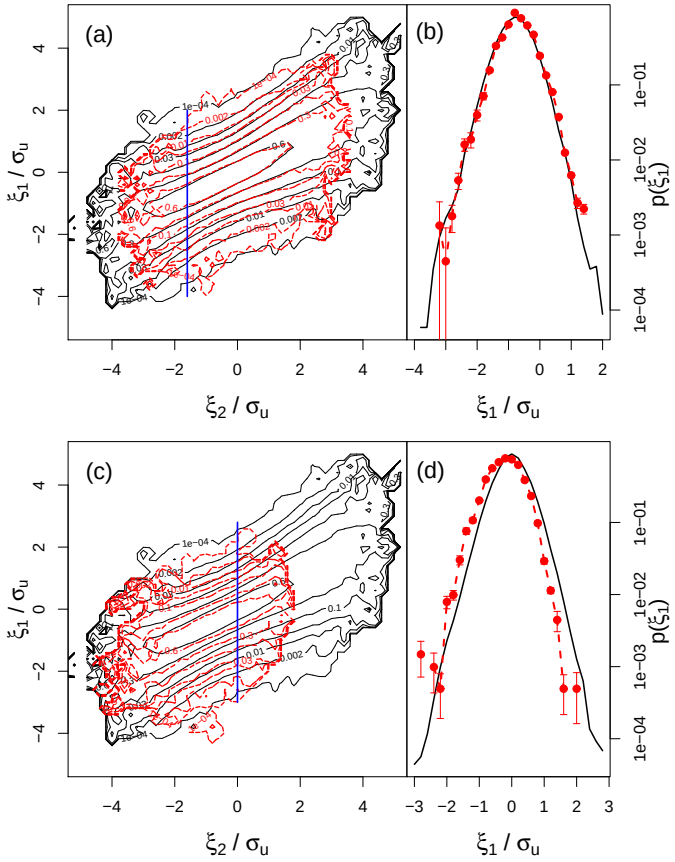

Figure 4.1: Contour plots of the conditional distributions $p(\xi_1|\xi_2)$ (black), and $p(\xi_1|\xi_2, u_i)$ (red), with $\xi_j \equiv \xi(r_j)$, for scales $r_1 = 2\lambda \approx L/4$, and $r_2 = 4\lambda \approx L/2$, for $u_i = 0 \pm \sigma_u/4$ (a), and $u_i = 2\sigma_u \pm \sigma_u/4$ (c). Figures (b) and (d) show cuts through the contour plots at fixed values of ξ_2 (along the vertical straight lines in figures (a) and (b), respectively). Free jet.

of different sizes have the same statistical distribution. Since the two distributions of (4.7) are necessarily of different sizes, the Wilcoxon test is an appropriate method to estimate its validity. The test is described in

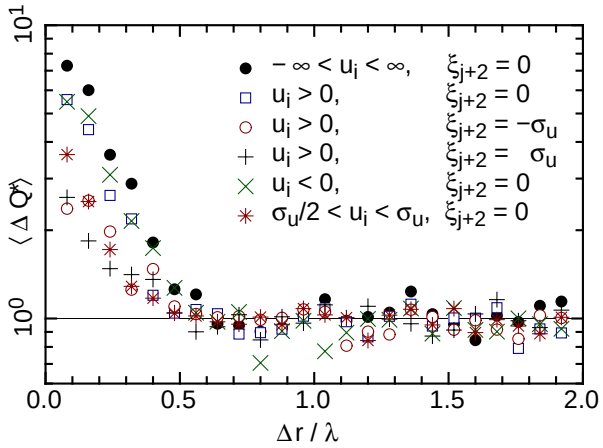

Figure 4.2: Wilcoxon test of (4.7) for different values of u_i and ξ_{j+2} as indicated in the legend ($\xi_{j+2} = 0$ is short for $\xi_{j+2} = 0 \pm \sigma_u/8$, and $\xi_{j+2} = (-)\sigma_u$ is short for $\xi_{j+2} = (-)\sigma_u \pm \sigma_u/6$). Cylinder wake at R_λ = 338.

detail in Section 4.5. Fig. 4.2 shows the results of the Wilcoxon test for (4.7) for different values of u_i and ξ_{j+2}. In the present implementation of the Wilcoxon test, a statistical test value $\langle \Delta Q^* \rangle$ is computed, which must be close to one for acceptance of the hypothesis expressed by (4.7). The values $\langle \Delta Q^* \rangle$ in Fig. 4.2 are in fact identical to one, except for some inevitable scattering, for large enough scale distances $\Delta r > l_{EM} \approx 0.6\lambda$. Thus, the Markov property of the interscale process is conserved under the additional condition of u_i, and (4.7) and (4.8) do apply.

The drift and diffusion functions of (4.12) for homogeneous isotropic turbulence are approximately linear and second-order functions in ξ, as was found previously in [18, 19]:

$$\tilde{D}^{(1)}(\xi, r) = -\tilde{d}_{11}(r)\xi, \tag{4.14}$$

$$\tilde{D}^{(2)}(\xi, r) = \tilde{d}_{20}(r) - \tilde{d}_{21}(r)\xi + \tilde{d}_{21}(r)\xi^2. \tag{4.15}$$

Here and for the remaining part of the paper, we skip the indices in ξ_j, r_j, and u_i for simplicity. The velocity increments ξ are given in units of their standard deviation in the limit $r \to \infty$, σ_∞, which is identical to $\sqrt{2}\sigma_u \equiv \sqrt{2\langle u^2 \rangle}$ [18]. This normalization allows a comparison of the

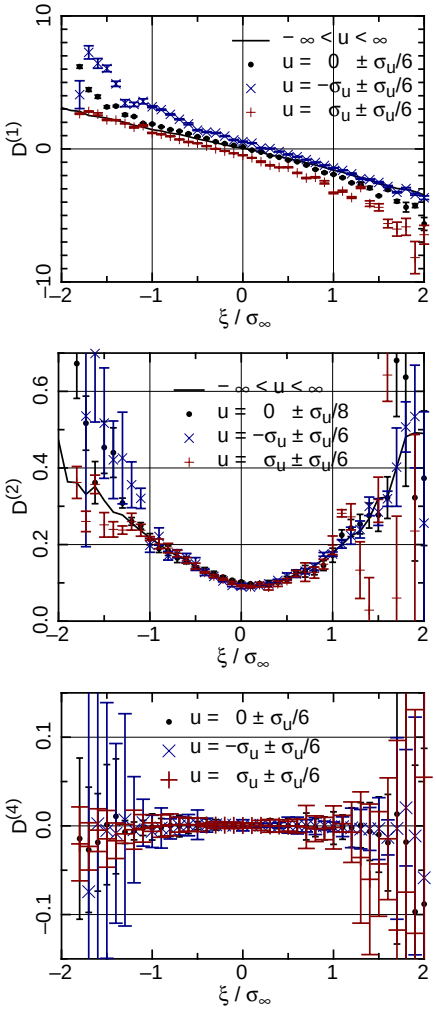

Figure 4.3: Drift and diffusion functions $D^{(1)}(\xi,r,u)$ and $D^{(2)}(\xi,r,u)$, and Kramers-Moyal coefficient $D^{(4)}(\xi,r,u)$ for different values of u. $D^{(1)}$ is shown for $r_j = 20\lambda$, $D^{(2)}$ and $D^{(4)}$ for $r = 3\lambda$. Cylinder wake at R_λ = 338.

Kramers-Moyal coefficients of different flows. As pointed out in [18], it is known that a diffusion function which is constant in ξ has Gaussian solutions, whereas the additional ξ-dependent terms present in (4.15) are responsible for intermittency effects and anomalous scaling of the structure functions.

In the following, we examine the velocity-dependence of the drift and diffusion functions. Fig. 4.3 shows exemplary drift functions $D^{(1)}(\xi,r,u)$ of the cylinder wake at R_λ = 338 for different values of u. For $u \neq 0$, the drift functions are essentially shifted in the vertical direction in comparison to the drift for $u = 0$, while their slopes do not depend visibly on u. The diffusion functions, also shown in Fig. 4.3, do not depend significantly on u. Furthermore, the fourth-order Kramers-Moyal coefficient $D^{(4)}(\xi,r,u)$ in Fig. 4.3 is zero within the estimation errors. Thus, the description of the stochastic process by a Fokker-Planck equation is valid, and the velocity-dependent drift and diffusion functions can be approximately described by first and second-order polynomials in ξ,

$$D^{(1)}(\xi,r,u) = d_{10}(r,u) - d_{11}(r)\xi, \tag{4.16}$$

$$D^{(2)}(\xi,r) = d_{20}(r) - d_{21}(r)\xi + d_{21}(r)\xi^2. \tag{4.17}$$

The most significant difference to (4.14) and (4.15) is the presence of the additional velocity-dependent term d_{10} in the drift function. The coefficient d_{10} is the leading velocity-dependent term, which can also be seen from the shift of the conditional PDFs in Fig. 4.1c-d.

The r-dependence of d_{10} for different values of u is shown in Fig. 4.4. For the cylinder wake and fractal grid in figures 4.4a and 4.4c, the dependences of d_{10} on both r and u are quite similar and approximately symmetric in u, $d_{10}(r,u) \approx -d_{10}(r,-u)$. In contrast, d_{10} is not symmetric in u for the free jet in Fig. 4.4b. In all cases, d_{10} can be approximated by a second-order polynomial in r,

$$d_{10}(r,u) = d_{101}(u)\frac{r}{\lambda} + d_{102}(u)\left(\frac{r}{\lambda}\right)^2. \tag{4.18}$$

The dependence of the coefficients d_{101} and d_{102} on the velocity u is shown in Fig. 4.5. We find that the parameters d_{101} and d_{102} depend on the flow geometry as well as on the Reynolds number. In the cases of the cylinder wake and fractal grid, the term d_{101} is almost linear in u for low Reynolds numbers, and becomes more S-shaped for higher Reynolds

numbers (figures 4.5a and 4.5c); the term d_{102} is approximately linear in u, with Reynolds number dependent slopes in the case of the cylinder wake (figures 4.5d and 4.5f). For the free jet, neither d_{101} nor d_{102} are linear in u, and d_{101} is also strongly asymmetric (figures 4.5b and 4.5e).

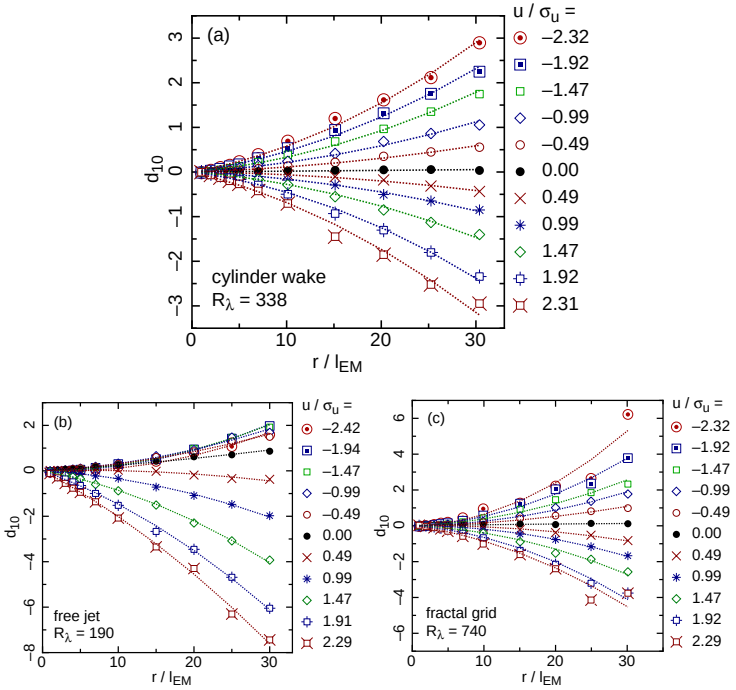

Figure 4.4: Coefficient d_{10} from (4.16) as function of r for different values of the velocity u, given in the legend. The dotted lines are fits according to (4.18). (a) cylinder wake at $R_\lambda = 338$, (b) free jet at $R_\lambda = 190$, (c) fractal square grid at $R_\lambda = 740$.

Fig. 4.6 shows the coefficients d_{11}, d_{20}, d_{21}, and d_{22} of (4.16) and (4.17) as functions of r for different values of u for the cylinder wake data at R_λ = 338. Reliable estimates of these coefficients for values of $|u| > \sigma_u$ can not be obtained due to the small number of available data for large velocity fluctuations. None of the coefficients shows a similarly systematic dependence on u as the coefficient d_{10} in Fig. 4.4.

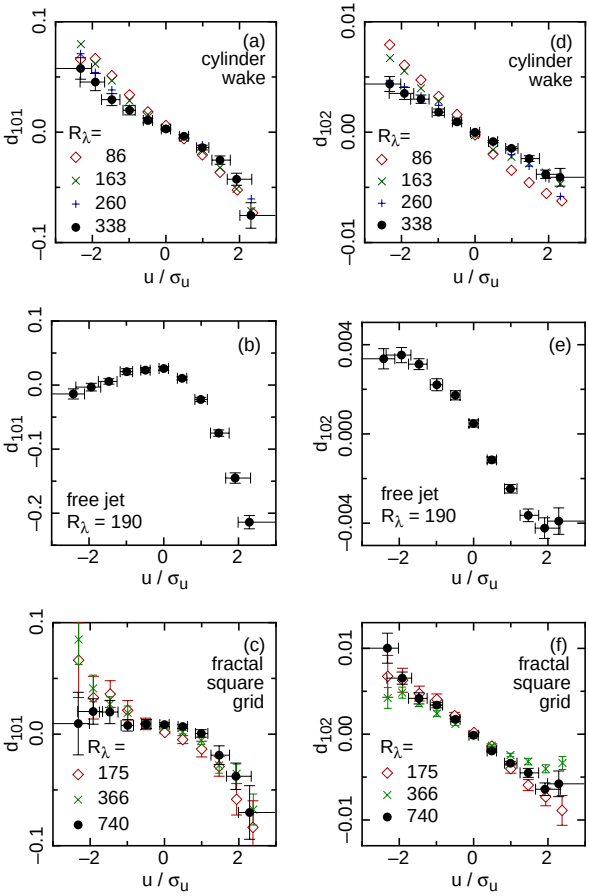

Figure 4.5: Coefficients d_{101} (a,b,c) and d_{102} (d,e,f) of the fits to d_{10}, according to (4.18), at different Reynolds numbers R_λ given in the legends. (a,d): cylinder wake, (b,e): free jet, (c,f): fractal square grid. The horizontal error bars shown for the highest Reynolds number data represent the range (bin size) of values of u used for the estimation of the drift. The vertical error bars are the errors of the estimated parameters d_{101} and d_{102}.

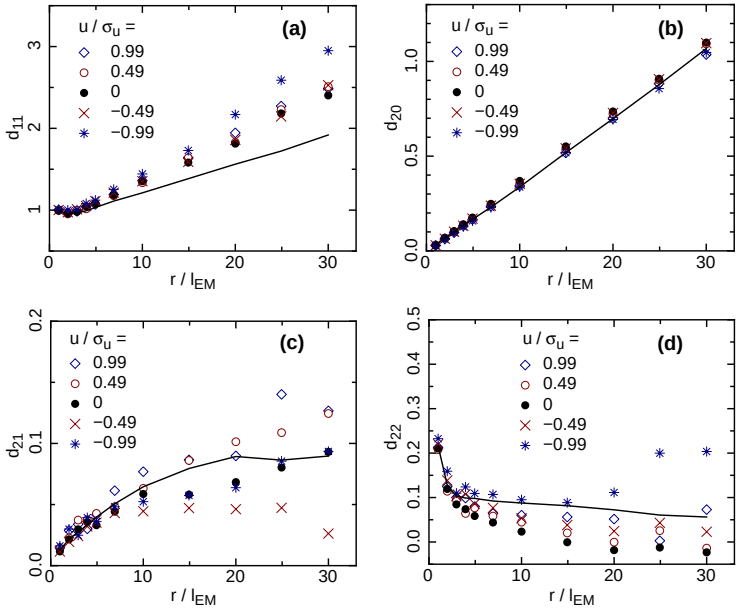

Figure 4.6: Coefficients d_{11}, d_{20}, d_{21}, and d_{22} from (4.16) and (4.17) as function of r for different values u, given in the legend. The solid lines represent the coefficients $\tilde{d}_{11}$, $\tilde{d}_{20}$, $\tilde{d}_{21}$, and $\tilde{d}_{22}$ from (4.14) and (4.15). Cylinder wake at R_λ = 338.

The slope d_{11} of the drift function only deviates for $u \approx -\sigma_u$ at large scales r, and the leading order coefficient of the diffusion function, d_{20}, practically does not depend on u at all. The coefficients d_{21} and d_{22} are scattered due to the large estimation errors, especially at large scales. Fig. 4.6d suggests that d_{22} decreases —and therefore the diffusion function $D^2(\xi)$ becomes flatter— for smaller values of $|u|$, which would correspond to a more Ornstein-Uhlenbeck-like process in the vicinity of u = 0. However, we should note that the dependences of d_{21} and d_{22} on u are relatively small at scales $r < 5\,l_{EM}$, and that these coefficients are more difficult to estimate than d_{10}, d_{11}, and d_{20}.

Fig. 4.6 also shows the coefficients $\tilde{d}_{11}$, $\tilde{d}_{20}$, $\tilde{d}_{21}$, and $\tilde{d}_{22}$ of (4.14) and (4.15) as solid lines. While the coefficients d_{20} and $\tilde{d}_{20}$ are identical

at all scales, the coefficients d_{11} and d_{22} are different from $\tilde{d_{11}}$ and $\tilde{d_{22}}$, respectively, at large scales r. The difference between the slopes of the drift functions, d_{11} and $\tilde{d_{11}}$ at large scales r can also be observed in Fig. 4.3.

4.4 Conclusions

It was found in [14] that the stochastic cascade process of velocity increments from scale to scale can be described by a Fokker-Planck equation. This description gives access to the joint multi-scale PDF $p[\xi(r_1),\xi(r_2),\ldots,\xi(r_N)]$ of the velocity increments ξ at the scales r_j. The structure functions $S_n(r) \equiv \langle \xi(r)^n \rangle$ can also be obtained from this description (see also [15, 17, 18, 19, 20, 21, 22]).

In the present paper we showed how this method can be extended in order to obtain the joint multi-point PDF $p[U(x_1),U(x_2),\ldots,U(x_N)]$ of the velocity U at the points x_i. This description is more complete than the multi-scale description, since it takes into account the velocity-dependence of the small-scale statistics. The multi-point statistics can be obtained from a Fokker-Planck equation for the conditional PDF $p[\xi(r_1)|\xi(r_2),u]$, where u is the fluctuating velocity. The Fokker-Planck equation follows from the Markov property of the underlying stochastic process and from the experimental observation that the fourth-order Kramers-Moyal coefficient can be neglected.

The Fokker-Planck equation for the multi-point statistics differs from the Fokker-Planck equation for the multi-scale statistics mainly by the presence of a simple additional term in the drift function. This term, $d_{10}(r,u)$, represents a vertical, velocity-dependent shift of the drift function. It implies that when, for example, $\xi(r_2) = 0$ and $u \gg 0$, then $\xi(r_1)$ at the scale $r_1 < r_2$ is likely to be negative. This is reasonable because $\xi(r_2)$ and $\xi(r_1)$ are to some extend independent and, loosely speaking, the increments have the tendency to drive the velocity signal back to zero, since it is stationary at large scales $r \gg L$. The shift of the drift function corresponds to the shift of the conditional PDF $p[\xi(r_1)|\xi(r_2),u]$, observed in Fig. 4.1.

It was found in previous works that the coefficients of the Fokker-Planck equation for the interscale process are not universal, but depend on the Reynolds number [19] and/or flow geometry [22]. We now found a similar result for the velocity-dependent coefficient d_{10}, which does

depend on the flow type and, at least in the case of the cylinder wake, also on the Reynolds number. On the basis of the examined data sets with lengths of up to 10^7, we can not make definite statements on the velocity-dependence of the other coefficients.

The coefficients of the Fokker-Planck equation can be estimated directly from the measured data. With the knowledge of these coefficients, the N-point statistics of the velocity field are given by the three-point statistics $p[u(x+r_1)|u(x+r_2),u(x)]$, which are equivalent to $p[\xi(r_1)|\xi(r_2),u(x)]$. Thus, a stochastic three-point closure for the turbulent velocity is given.

The analysis presented in the present paper is restricted to a single velocity component, but in principle, it can be extended to a velocity vector with three components. The drift and diffusion functions would then become tensors $D_i^{(1)}(\boldsymbol{\xi},r,\mathbf{u})$ and $D_{ij}^{(2)}(\boldsymbol{\xi},r,\mathbf{u})$, which contain coupling terms between the different velocity (increment) components. Siefert *et al.* [21] investigated the Fokker-Planck equation for two components of the velocity increment $\boldsymbol{\xi}$, and found that the drift function decouples, while the diffusion function contains non-vanishing coupling terms between longitudinal and transversal velocity increments. These coupling terms were found to have simple functional forms, and thus the analysis can be easily extended to more than one velocity component. However, such an analysis requires more data —Siefert *et al.* [21] needed data of length 10^8 to perform the two-dimensional analysis *without* conditioning on the velocity— and is therefore left to future studies. With the knowledge of (or appropriate assumptions about) the coupling coefficients, it would be possible to extend the method of time-series generation proposed in [23, 24] —with the additional conditioning on the velocity proposed in the present paper—, to the generation of synthetic turbulent velocity signals with three components.

We thank S. Lück, C. Renner, and J. C. Vassilicos for the experimental data, and acknowledge financial support by DFG Grant No. PE 478/14-1.

4.5 Appendix: The (Mann-Whitney-)Wilcoxon test

The null hypothesis to be tested by the Wilcoxon test [29, 30, 18] is that the probability density functions $p(x)$ and $\tilde{p}(y)$ of the stochastic variables x and y are identical. In the case of Eq. (4.3), for example, the two stochastic variables are $x = \xi_j|_{\xi_{j+1}}$, and $y = \xi_j|_{\xi_{j+1},\xi_{j+2}}$. Two samples $x_1,...,x_N$ and $y_1,...,y_M$ of independent realizations of the variables are taken from the data. We take values which are separated by one integral length to be sufficiently independent from each other for the purpose of the test, in order not to reduce the sample sizes too much. Then, the number of values x_n with $x_n < y_m$ is counted for each y_m and summed over m:

$$Q = \sum_{m=1}^{M} \sum_{n=1}^{N} z_{mn}, \quad z_{mn} = \begin{cases} 1 : x_n < y_m \\ 0 : x_n \geq y_m \end{cases} . \tag{4.19}$$

Under the null hypothesis, the quantity Q is Gaussian distributed with mean value $\mu_0(N,M) = NM/2$, and, for $N,M > 25$, standard deviation $\sigma_0(N,M) = \sqrt{NM(N+M+1)/12}$. Also under the null hypothesis, it follows that the quantity

$$\Delta Q = \frac{|Q - \mu_0(N,M)|}{\sigma_0(N,M)}, \tag{4.20}$$

which is the absolute value of a standard normal distributed variable, has a mean value of $\sqrt{2/\pi}$. In the present implementation of the test, the quantity

$$\Delta Q^* \equiv \Delta Q / \sqrt{2/\pi} \tag{4.21}$$

is calculated for a fixed value of ξ_{j+2} for a number of 100 bins for ξ_{j+1}, which span the complete range of ξ_{j+1}. The mean value $\langle \Delta Q^* \rangle$ is calculated by taking the average over the 100 values of ΔQ^*. Under the null hypothesis of Markov properties, the expectation value of ΔQ^* is one.

Bibliography

[1] U. Frisch. *Turbulence – The legacy of A. N. Kolmogorov*. Cambridge University Press, 1995.

[2] A. A. Praskovsky, E. B. Gledzer, M. Y. Karyakin, and Y. Zhou. The sweeping decorrelation hypothesis and energy-inertial scale interaction in high Reynolds number flow. *J. Fluid Mech.*, 248:493–511, 1993.

[3] K. R. Sreenivasan and G. Stolovitzky. Statistical dependence of inertial range properties on large scales in a high-Reynolds-number shear flow. *Phys. Rev. Lett.*, 77:2218–2221, 1996.

[4] K. R. Sreenivasan. Possible effects of small-scale intermittency in turbulent reacting flows. *Flow Turb. Comb.*, 72:115–131, 2004.

[5] I. Hosokawa. A paradox concerning the Refined Similarity Hypothesis of Kolmogorov for isotropic turbulence. *Prog. Theor. Phys.*, 118:169–173, 2007.

[6] G. Parisi and U. Frisch. On the singularity structure of fully developed turbulence. In M. Ghil, R. Benzi, and G. Parisi, editors, *Turbulence and Predictability in Geophysical Fluid Dynamics, Proceed. Intern. School of Physics 'E. Fermi', 1983, Varenna, Italy*, pages 84–87. North–Holland, Amsterdam, 1985.

[7] B. B. Mandelbrot. Intermittent turbulence in self similar cascades; divergence of high moments and dimension of the carrier. *J. Fluid Mech.*, 62, 1997.

[8] B. B. Mandelbrot. *Fractals and Scaling in Finance: Discontinuity, Concentration, Risk*. Springer Verlag, 1997.

[9] B. B. Mandelbrot, A. Fisher, and L. Calvet. A multifractal model of asset returns. *Cowles Foundation Discussion Paper No. 1164*, 1997.

[10] E. Bacry, J. Delour, and J. F. Muzy. Multifractal random walk. *Phys. Rev. E*, 64:026103, 2001.

[11] M. I. Bogachev, J. F. Eichner, and A. Bunde. Effect of nonlinear correlations on the statistics of return intervals in multifractal data sets. *Phys. Rev. Lett.*, 99:240601, 2007.

[12] M. I. Bogachev and A. Bunde. Improved risk estimation in multifractal records: Application to the value at risk in finance. *Phys. Rev. E*, 80:026131, 2009.

[13] V. Yakhot. Probability densities in strong turbulence. *Physica D*.

[14] R. Friedrich and J. Peinke. Description of a turbulent cascade by a Fokker-Planck equation. *Phys. Rev. Lett.*, 78:863–866, 1997.

[15] R. Friedrich and J. Peinke. Statistical properties of a turbulent cascade. *Physica D*, 102:147–155, 1997.

[16] S. Lück, C. Renner, J. Peinke, and R. Friedrich. The Markov–Einstein cohernce length—a new meaning for the Taylor length in turbulence. *Phys. Lett. A*, 359:335–338, 2006.

[17] R. Friedrich, J. Zeller, and J. Peinke. A note on three-point statistics of velocity increments in turbulence. *Europhys. Lett.*, 41:153–158, 1998.

[18] C. Renner, J. Peinke, and R. Friedrich. Experimental indications for Markov properties of small-scale turbulence. *J. Fluid Mech.*, 433:383–409, 2001.

[19] C. Renner, J. Peinke, R. Friedrich, O. Chanal, and B. Chabaud. Universality of small scale turbulence. *Phys. Rev. Lett.*, 89:124502, 2002.

[20] M. Tutkun and L. Mydlarski. Markovian properties of passive scalar increments in grid-generated turbulence. *New J. Phys.*, 6:49, 2004.

[21] M. Siefert and J. Peinke. Different cascade speed for longitudinal and transverse velocity increments of small-scale turbulence. *Phys. Rev. E*, 70:015302, 2004.

[22] R. Stresing, J. Peinke, R. E. Seoud, and J. C. Vassilicos. Defining a new class of turbulent flows. *Phys. Rev. Lett.*, 104(19):194501, 2010.

[23] A. P. Nawroth and J. Peinke. Small scale behavior of financial data. *Eur. Phys. J. B*, 50:147–150, 2006.

[24] A. P. Nawroth, R. Friedrich, and J. Peinke. Multi-scale description and prediction of financial time series. *New J. Phys.*, 12:083021, 2010.

[25] R. Friedrich R. Stresing, D. Kleinhans and J. Peinke. Different methods to estimate the einstein-markov coherence length in turbulence. *Phys. Rev. E*, page submitted.

[26] H. Risken. *The Fokker-Planck Equation*. Springer Verlag, 1996.

[27] S. Lück. *Turbulente Nachlaufströmungen*. Der Andere Verlag, Tönning, 2001.

[28] R. E. Seoud and J. C. Vassilicos. Dissipation and decay of fractal-generated turbulence. *Phys. Fluids*, 19:105108, 2007.

[29] F. Wilcoxon. Individual comparisons by ranking methods. *Biometrics Bull.*, 1(6):80–83, 1945.

[30] H. B. Mann and D. R. Whitney. On a test of whether one of two random variables is stochastically larger than the other. *Ann. Math. Stat.*, 18:50–60, 1947.

Chapter 5

Further Results

5.1 Multi-point correlations in inhomogeneous turbulence[1]

Abstract We examine the spatial Markov properties of all three velocity components in inhomogeneous turbulence. We use measurement data of the axisymmetric far wake behind a disk at $Re = 2 \cdot 10^4$, measured simultaneously with cross hot wire probes at twelve different distances from the flow axis. We show that the velocity components and Reynolds stresses can be approximated by Markov processes for large enough separations perpendicular to the flow direction. Our results indicate that the N-point correlations of the velocity components and the Reynolds-stresses in inhomogeneous turbulence might be approximated by a stochastic process governed by a Fokker-Planck equation, which could be the basis of a stochastic closure of the Reynolds averaged Navier-Stokes equations.

[1] This Section 5.1 has been published as R. STRESING, M. TUTKUN, and J. PEINKE, Spatial multi-point correlations in inhomogeneous turbulence *in* J. PEINKE, M. OBERLACK, and A. TALAMELLI (eds.), *Progress in Turbulence III – Proceedings of the iTi Conference in Turbulence 2008*, Springer, 2009. The mathematical notation has been slightly modified.

5.1.1 Introduction: Closure problem and stochastic processes

The central problem of turbulence is to determine the n-point probability density functions (PDF) of the velocity field. One mathematical formulation of this problem is the infinite Friedmann-Keller system of differential equations for all possible moments of these PDFs [1]. Any finite subsystem of this system is always unclosed, as, for example, are the Reynolds averaged Navier-Stokes (RANS) equations:

$$\frac{\partial \rho \bar{u_i}}{\partial t} + \frac{\partial}{\partial x_j}\left(\rho \bar{u_i}\bar{u_j} + \rho \overline{u_i' u_j'}\right) = -\frac{\partial \bar{p}}{\partial x_i} + \rho \nu \nabla^2 \bar{u_i}, \tag{5.1}$$

where the velocity components have been split into their mean and fluctuating parts, $u_i = \bar{u_i} + u_i'$.[2] Turbulence models based on the RANS equations focus on expressions for the Reynolds stresses $\tau_{ij} = -\rho \overline{u_i' u_j'}$. We propose a solution based on stochastic process equations for the Reynolds stresses.

If the PDFs of the Reynolds stresses, $p(u_i' u_j')$, or the joint PDF of the fluctuations, $p(u_1', u_2', u_3')$, are known, the Reynolds stresses can be calculated:

$$\overline{u_i' u_j'} = \int_{-\infty}^{\infty} u_i' u_j'\, p(u_i' u_j')\, \mathrm{d}u_i' u_j' = \int_{-\infty}^{\infty}\int_{-\infty}^{\infty}\int_{-\infty}^{\infty} u_i' u_j'\, p(u_1', u_2', u_3')\, \mathrm{d}u_1' \mathrm{d}u_2' \mathrm{d}u_3'. \tag{5.2}$$

We want to know the N-point joint PDFs of the components of the velocity fluctuations or the Reynolds stress tensor, $p[\phi(r_N), \ldots, \phi(r_1)]$, where ϕ stands for u_i or τ_{ij}, and the points r_n are assumed to be equally spaced and lie on a straight line. If the stochastic process for the spatial evolution of the quantity ϕ has Markov properties, that is, if

$$p[\phi(r_n)|\phi(r_{n-1}), \ldots, \phi(r_1)] = p[\phi(r_n)|\phi(r_{n-1})], \tag{5.3}$$

the N-point joint PDF of can be expressed by a product of conditional PDFs:

$$p[\phi(r_N), \phi(r_{N-1}), \ldots, \phi(r_1)] = p[\phi(r_N), \phi(r_{N-1})] \ldots p[\phi(r_2), \phi(r_1)] p[\phi(r_1)]. \tag{5.4}$$

[2] [Only within the present section the index i in u_i denotes the i-th *component* of the velocity vector.]

The stochastic process for the conditional PDFs can be described by a Kramers-Moyal expansion. If the fourth-order Kramers-Moyal coefficient $D^{(4)}$ is zero, the expansion truncates after the second term[3] and becomes a Fokker-Planck equation:[4,5]

$$\frac{\partial}{\partial r}p(\phi,r|\phi_0,r_0) = \left[-\frac{\partial}{\partial\phi}D^{(1)}(\phi,r) + \frac{\partial^2}{\partial\phi^2}D^{(2)}(\phi,r)\right] p(\phi,r|\phi_0,r_0), \tag{5.5}$$

which is equivalent to the corresponding Langevin equation (Itō formalism) for the quantity $\phi(r)$ itself:

$$\frac{\partial}{\partial r}\phi(r) = D^{(1)}(\phi,r) + \sqrt{D^{(2)}(\phi,r)}\,\Gamma(r), \tag{5.6}$$

where $\Gamma(r)$ represents Gaussian white noise, and the drift and diffusion functions $D^{(1)}$ and $D^{(2)}$ are defined as:

$$D^{(k)}(\phi,r) = \lim_{\Delta r\to 0}\frac{1}{k!\Delta r}\int_{-\infty}^{+\infty}(\tilde{\phi}-\phi)^k\, p(\tilde{\phi},r-\Delta r|\phi,r)\,\mathrm{d}\tilde{\phi}. \tag{5.7}$$

Note that averaging over Eq. (5.6) for $\phi = \tau_{ij}$ and $r = x_j$ gives an expression for the term $\frac{\partial}{\partial x_j}\overline{u_i'u_j'}$ in Eq. (5.1)[6].

5.1.2 Experimental results – Markov properties

As an example for an inhomogeneous turbulent flow we analyze cross hot-wire measurements in the axisymmetric wake of a disc with diameter D = 20 mm, taken simultaneously at twelve distances r_i from the flow axis at a downstream distance $x/\mathrm{D} = 50$, at Reynolds number $Re = \mathrm{U}_\infty\mathrm{D}/\nu = 20\,400$ [6]. We denote the component of the velocity fluctuations in the direction of the main flow as u, the transverse compontent as v, and the azimuthal (tangential) component as w. We

[3] Pawula's theorem states that if $D^{(4)} = 0$, then $D^{(k)} = 0$ for all $k > 2$.

[4] The present work is based on previous investigations of the *N-scale* joint PDFs of the velocity *increments* on different scales [2, 3, 4, 5]. It has been shown for several different flow types over a wide range of Reynolds numbers, that the scale-to-scale evolution of the PDFs of the increments can be described by a Fokker-Planck equation.

[5] For simplicity, we write ϕ and ϕ_0 instead of $\phi(r_n)$ and $\phi(r_{n-1})$ in Eq. (5.5) to Eq. (5.7).

[6] Incompressibility is assumed and ρ is omitted.

only look at the three probe positions closest to the axis of the disk: $r_1 = 0.67\,\delta_*$, $r_2 = \delta_*$, and $r_3 = 1.33\,\delta_*$, where r is zero on the axis, and $\delta_* = 42$ mm is the transverse length scale. The Integral length in the direction of u is $L_u = 23$ mm at r_1 (inner position), and $L_u = 43$ mm at r_3 (outer position).

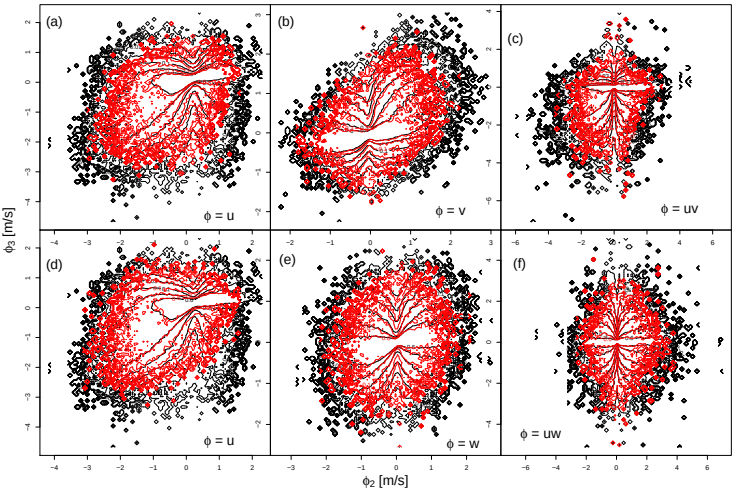

Figure 5.1: Contour plots of $p[\phi(r_3)|\phi(r_2)]$ (black) and $p[\phi(r_3)|\phi(r_2),\phi(r_1)]$ (red), with (a,d) $\phi = u$, (b) $\phi = v$, (c) $\phi = uv$, (e) $\phi = w$, and (f) $\phi = uw$. In all plots, $\phi(r_1) = 0 \pm \sigma_\phi/8$, except in (d), where $\phi(r_1) = -1 \pm \sigma_\phi/6$.

We examine the Markov properties of the measurement data by a graphical inspection of both sides of

$$p[\phi(r_3)|\phi(r_2),\phi(r_1)] = p[\phi(r_3)|\phi(r_2)], \tag{5.8}$$

which is a simplification of Eq. (5.3), sufficient for finite data sets. Fig. 5.1 shows the right and left hand sides of Eq. (5.8), where $\phi(r_n)$ stands for the variables u, v, w, uv, and uw at the position r_n.

In all cases, the general shapes of the conditional PDFs of Eq. (5.8) agree very well. There are some minor differences especially around $\phi(r_2) = 0$ (the "notch" in the PDFs), which increase as $\phi(r_1)$ deviates from zero, as can be seen from figures (a) and (d) for the case of $\phi = u$.

These differences around $\phi(r_2) = 0$ can be explained by the presence of more quiescent, or quasi-laminar phases of the flow, which do not have Markov properties.

Having shown that the data has approximate Markov properties for sufficiently large spatial separations, we can state that the stochastic process for $\frac{\partial}{\partial r} p[\phi(r_n)|\phi(r_{n-1})]$ can be approximated by a Kramers-Moyal expansion. If, furthermore, the fourth-order Kramers-Moyal coefficient is zero, the process follows a Fokker-Planck equation. As we cannot calculate the (spatial) Kramers-Moyal coefficients directly from our data, this problem is left for future studies on the basis of multi-point measurements with smaller separations Δr, or on the basis of numerical simulations.

We conclude that the N-point statistics of inhomogeneous turbulence in the wake of a disk can be approximated by a Markov process. This result indicates that the spatial derivatives of the Reynolds stresses can be described by a stochastic process, possibly governed by a Fokker-Planck equation.

5.2 Further results on fractal-generated turbulence

For lack of space, the following result obtained for fractal-generated turbulence was not included in the publication which is presented as Chapter 2 of this book.

5.2.1 Coefficients d_{21} and d_{22}

The coefficients d_{22}, and especially d_{21} of Eq. (2.6) from Chapter 2 are more difficult to estimate than the leading coefficients d_{11} and d_{20}, and they are also less important for the stochastic process. Figure 5.2 shows that the coefficient $d_{21}(r)$ displays a dependency on the Reynolds number R_λ for fractal-generated turbulence, when estimated directly from Eq. (2.4). This systematic dependency is not present for the optimized coefficient in the lower part of the figure. In the case of the coefficient $d_{22}(r)$, it is not clear weather there is a systematic dependency on R_λ, or just strong scattering. The optimized coefficient d_{22} does not — or only very weakly — depend on R_λ. Although there might be some dependence of the directly estimated coefficient d_{21} on R_λ, the optimized coefficients d_{21} and d_{22} do not depend on R_λ. This observation confirms our result that the Fokker-Planck equation for the interscale process of fractal-generated turbulence is independent of the Reynolds number.

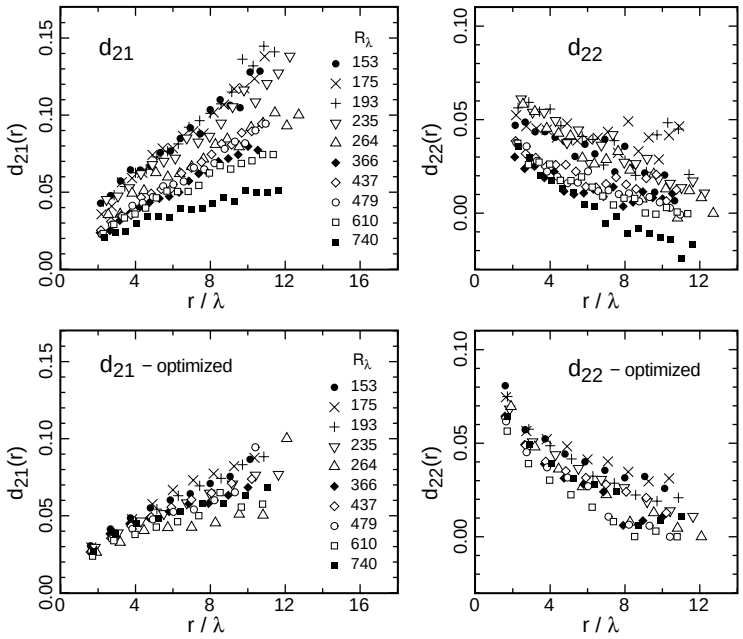

Figure 5.2: Coefficients d_{21} and d_{22} of Eq. (2.6) as functions of the scale r for the fractal square grid, estimated directly (upper figures) and by numerical optimization (lower figures). Reynolds numbers R_λ are given in the legends.

5.3 Further results on Markov properties of turbulence

This section should be read in context with, and as a supplement to, Chapter 3.

5.3.1 Dependence of the Fokker-Planck equation on the nesting structure of velocity increments

In Section 3.2.2, we investigated the Markov property of the stochastic processes in scale for different nesting structures of the velocity increments. We found that the Einstein-Markov coherence length is similar for different nesting structures, if an appropriate measure for the distance between scales is applied. In the present Section, we want to examine how the coefficients of the Fokker-Planck equation depend on the nesting structure.

The drift and diffusion functions of the Fokker-Planck equation (3.4) can be estimated from the conditional moments $M^{(k)}(\xi, r, \Delta r)$,

$$D^{(k)}(\xi, r) = \lim_{\Delta r \to 0} M^{(k)}(\xi, r, \Delta r) \tag{5.9}$$

$$\begin{aligned} M^{(k)}(\xi, r, \Delta r) &= \frac{r_j}{k! \Delta r} \langle \left[\xi'(r - \Delta r) - \xi(r) \right]^k \rangle \\ &= \frac{r_j}{k! \Delta r} \int_{-\infty}^{\infty} (\xi' - \xi)^k \, p\left[\xi'(r - \Delta r) | \xi(r) \right] d\xi'. \end{aligned} \tag{5.10}$$

The extrapolation $\Delta r \to 0$ is usually performed by a linear fit to the values of $M^{(k)}(\xi, r, \Delta r)$ in the range $l_{EM} \leq \Delta r \leq 2 l_{EM}$ [4, 5]. Fig. 5.3(a) shows that this procedure would lead to very different estimates of the Kramers-Moyal coefficients $D^{(2)}(\xi, r)$. In contrast, if the linear fit is performed in the range $l_{EM} \leq \delta r \leq 2 l_{EM}$, where δr is defined as $\delta r = (\frac{1}{2} + |q - \frac{1}{2}|) \Delta r$ (see Section 3.2.2), the estimates of $D^{(2)}(\xi, r)$ are very similar, as shown in Fig. 5.3(b).[7] For the Einstein-Markov coherence length l_{EM}, we take the estimates for left-bounded increments, l_{EM}^l, and for centered increments, l_{EM}^c, respectively, from Table 3.1. It is also clear from the shapes of the graphs in Fig. 5.3(a) and (b) that the moments $M^{(2)}(u, r, \Delta r)$ for left-bounded and centered increments exhibit a

[7] For left-bounded increments ($q = 0$), the two measures are identical, $\delta r = \Delta r$, while for centered increments ($q = 1/2$), it is $\delta r = \Delta r / 2$.

similar scaling with δr and not with Δr. Thus, the extrapolation $\Delta r \to 0$ should be performed by a fit in the range $l_{EM}^{c/l} \leq \delta r \leq 2l_{EM}^{c/l}$.

After estimating the drift and diffusion functions by the linear fits shown in exemplary cases in Fig. 5.3(b), the drift and diffusion functions can be parameterized as

$$D^{(1)}(\xi, r) = -d_{11}(r)\xi, \tag{5.11}$$

$$D^{(2)}(\xi, r) = d_{20}(r) - d_{21}(r)\xi + d_{22}(r)\xi^2. \tag{5.12}$$

The estimated coefficients d_{ij} are shown as functions of r in Fig. 5.4. The leading coefficients d_{11} and d_{20} are practically identical for left-bounded and centered velocity increments. Only the coefficients d_{21} and d_{22} of the diffusion function depend significantly on the nesting structure. These coefficients, however, can not be estimated as precisely as d_{11} and d_{20}.

In conclusion, we note that when the drift and diffusion functions are estimated with a method based on the distance measure δr defined in Section 3.2.2, significant differences between left-bounded and centered nesting of velocity increments are only observed for the linear and quadratic terms of the diffusion function.

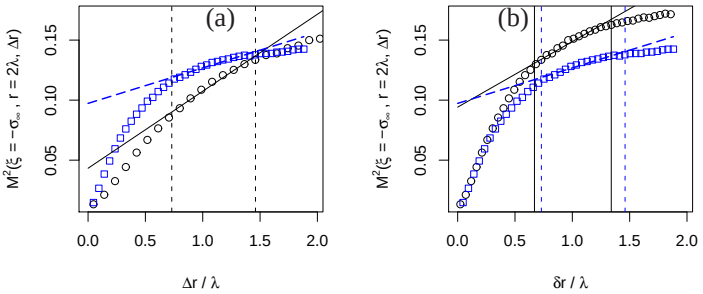

Figure 5.3: Coefficient $M^{(2)}(u,r,\Delta r)$ for $u=-\sigma_\infty$ and $r=2\lambda$ for the free-jet data at $R_\lambda = 190$. (Here, $\sigma_\infty = \sqrt{2}\sigma_u$, and σ_u is the standard deviation of the velocity.) The values for centered increments (circles), and left-bounded increments (squares) are plotted as functions of $\Delta r/\lambda$ (a), and $\delta r/\lambda$ (b). Linear fits for the determination of $D^{(2)}(u,r)$ are shown as straight lines for centered increments and dashed lines for left-bounded increments. Vertical lines denote the corresponding fit regions, $l^l_{EM} \le \Delta r \le 2l^l_{EM}$ in (a), and $l^c_{EM} \le \delta r \le 2l^c_{EM}$ for centered increments (straight lines), respectively $l^l_{EM} \le \delta r \le 2l^l_{EM}$ for left-bounded increments (dashed lines) in (b).

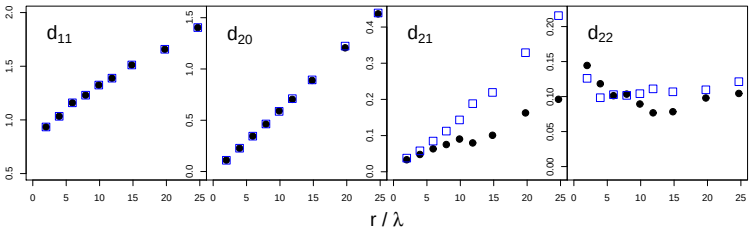

Figure 5.4: Estimated coefficients d_{ij} of Eq. (5.11) and (5.12) for the free-jet at $R_\lambda = 190$. Filled circles: centered increments; open squares: left-bounded increments.

5.3.2 Markov properties of synthetic data[8]

In this section, we examine if the observed Markov properties for the different processes (in time/space and in scale, and for different nesting structures of increments) are a specific feature of turbulence, or otherwise a more general phenomenon. Therefore, we analyze data generated by a non-Markovian stochastic process defined by

$$\mathrm{d}X_t = -\alpha X_t \mathrm{d}t + \mathrm{d}Y_t, \tag{5.13}$$

$$\mathrm{d}Y_t = -\beta Y_t \mathrm{d}t + \mathrm{d}W_t, \quad W_t - W_s \sim N(0, t-s), \tag{5.14}$$

where W_t is a Wiener process, and α and β are constants with $0 < \alpha < 1$ and $0 < \beta < 1$. Equation (5.13) is identical to an Ornstein-Uhlenbeck process, except that its noise Y_t is again generated by an Ornstein-Uhlenbeck process, defined by Eq. (5.14) ("colored noise").[9] The process defined by Equations (5.13) and (5.14) has no Markov property for any step size τ. Nevertheless, the conditional PDF $p(X_t|X_{t-\tau}, X_{t-2\tau})$ becomes *practically* independent of $X_{t-2\tau}$ for large enough τ in the sense that the dependence of the PDF on $X_{t-2\tau}$ is not statistically significant for large enough τ for finite synthetically generated time series.

For the 16 combinations of the values 0.05, 0.1, 0.2, and 0.3 for the parameters α and β, we generate discrete time series with step size $\tau = t_m - t_{m-1} = 1$ and length 10^6, which is comparable to the lengths of the experimental data examined in Chapter 3. We observe an exponential decay of the test value $\langle \Delta Q^* \rangle$ of the Wilcoxon test (see Section 3.5), which allows us to determine the *Einstein-Markov coherence length* by the same fitting method as for the experimental data. As base-increment length r_1 of the interscale processes we take half the integral length of the respective data, $r_1 = L/2$ (the ratios of L/l^l_{EM} vary between 1.4 and 3.2). The results are remarkably similar to those obtained for the turbulence data in Table 3.1: the ratios of the different length scales are $l^{ts}_{EM}/l^l_{EM} = 0.99 \pm 0.07$ and $l^c_{EM}/l^l_{EM} = 0.94 \pm 0.07$, where $l^c_{EM} \equiv \delta r^*$, as explained in Section 3.2.2.

Thus, the similarity of the Markov-Einstein coherence lengths for processes in space/time and in scale is not a special feature of turbu-

[8] Sections 5.3.2 and 5.3.3 are based on suggestions by David Kleinhans, whom I would like to thank for sharing his ideas.

[9] The Ornstein-Uhlenbeck process is the continuous-time analog of an autoregressive process of order one, AR(1).

lence, but it can also be observed for synthetically generated data like those examined in the present section.

5.3.3 Embedded Markov chain model

Kaminsky et al. [7] analyze non-stationary boundary-layer wind speed data with the one-step Markov chain model described in Section 3.3. In contrast to our results for stationary laboratory turbulence, the model fails completely to reproduce the power spectrum of the wind speed data. However, the power spectrum can be reproduced much better by a two-step *embedded* Markov chain model [7]. In this subsection, we apply such a model to our data in order to see if it is also capable of reproducing the inertial range intermittency and skewness of the increment distributions of stationary laboratory turbulence.

The embedded Markov chain model is a two-step procedure. First, a large-scale transition matrix is calculated for the velocities averaged over m elementary time steps τ. These averaged velocities are denoted U in the following. Next, a small-scale transition matrix for the elementary time step τ is calculated for the fluctuations around the average velocity values, $u'_t = u^*_t - U_t$. As in the one-step model described in Section 3.3, the time series are reduced to a number of discrete values of the velocities u^*, U, and, consequently, u'. In order to exclude 'jumps' in the time series, only transitions within the same level of U are considered for the calculation of the small-scale transition matrix. For the synthetic reconstruction of data, two time series are generated and added, one from the small-scale and one from the large-scale transition matrix (in the latter case, of course, each velocity value U is repeated m times).

We apply this two-step procedure to the cryogenic helium jet data at R_λ = 352, again for a basic step size τ equivalent to the Taylor microscale, $\tau = \lambda/\overline{u}$. The best results were achieved for a large scale transition matrix for step sizes in the order of the integral length, $L \approx 14.5\lambda$. Figure 5.5 shows the power spectrum of the reconstructed data for $m = 15$ together with the original and one-step model power spectra. The power spectrum of the embedded model is still closer to the original spectrum than the spectrum of one-step model in the low frequency range, but displays more deviations from the original data and cyclical fluctuations for high frequencies. The skewness of the increment distributions reflected in the third order structure function shown in figure 5.6

is more realistic for the embedded model than for the one-step model, but still reaches only about half the value of the original data. The values of flatness of the increment distributions shown in figure 5.6 are closer to the original data for the two-step model than for the one-step model for medium scales, but they exhibit sharp bends at the scale $m\lambda$, and multiples of $m\lambda$, and they are too large at small scales.

We conclude that the missing long-wave information of the one-step Markov chain model described in Section 3.3 can not be completely recovered by the two-step embedded Markov chain model. Such embedded models might be useful for the synthetic generation of wind speed data, where the reconstruction of the power spectrum is improved in comparison to the one-step model [7], but they are too simple to reproduce the intermittency and skewness of homogeneous isotropic turbulence.

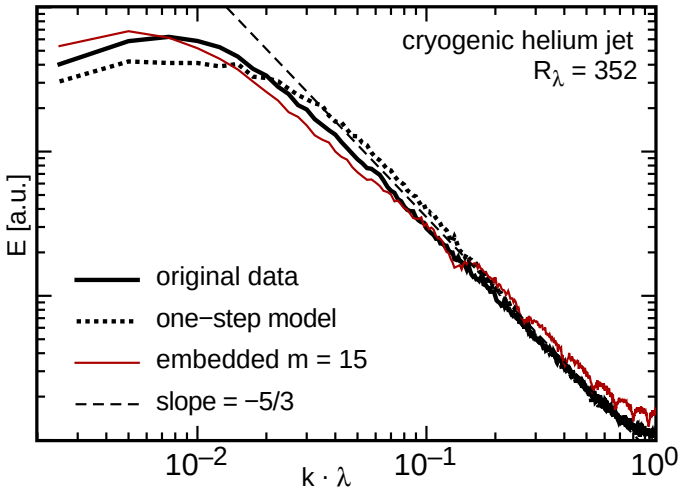

Figure 5.5: Power spectra of the original and reconstructed data for the cryogenic helium jet at R_λ = 352.

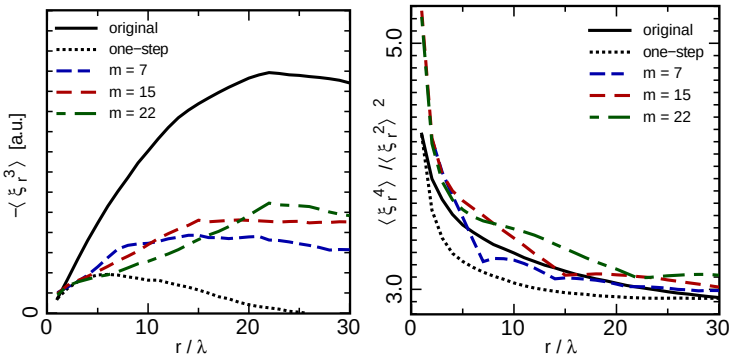

Figure 5.6: Third order structure functions and flatnesses of the velocity increment distributions of the original and reconstructed data for the cryogenic helium jet at R_λ = 352. The parameter m, which denotes the ratio of the large to the small scale of the transition matrices in the embedded model, is given in the legends.

5.4 Further results on multi-point statistics of turbulence

This section should be read in context with, and as a supplement to, Chapter 4.

5.4.1 Synthetically generated data

In order to get a better understanding of the relation between N-scale and (N+1)-point statistics, we analyze synthetic data generated by an autoregressive process of first order, AR(1),

$$u_i = \rho u_{i-1} + \varepsilon_i, \qquad \varepsilon_i \sim i.i.d.\mathrm{N}(0,1), \tag{5.15}$$

where ε_i is delta-correlated Gaussian white noise with mean zero and variance one,[10] and ρ is a real number between zero and one. For $\rho = 0$ the process is just white noise, and for $\rho = 1$ it is a random walk. The conditional density $p(\xi_1|\xi_2, u_i)$ can be calculated analytically from the transition probabilities

$$p(u_i|u_{i-1}) = \frac{1}{\sigma\sqrt{2\pi}} \exp\left[-\frac{(u_i - \rho u_{i-1})^2}{2\sigma^2}\right], \tag{5.16}$$

using

$$\begin{aligned} p(\xi_1|\xi_2, u_i) = \frac{p(\xi_1, \xi_2, u_i)}{p(\xi_2, u_i)} &= \frac{p(u_{i+2}, u_{i+1}, u_i)}{p(u_{i+2}, u_i)} \\ &= \frac{p(u_{i+2}|u_{i+1})p(u_{i+1}|u_i)}{\int_{-\infty}^{\infty} p(u_{i+2}|u_{i+1})p(u_{i+1}|u_i)du_{i+1}}. \end{aligned} \tag{5.17}$$

Assuming that $u_{i-1} = 0$, the solution is

$$\begin{aligned} p(\xi_1|\xi_2, u_i) &= p(u_{i+1}|u_{i+2}, u_i) \\ &= \sqrt{1+\rho^2} \exp\left[-\frac{1+\rho^2}{2\sigma^2}\left(u_{i+1} - \frac{\rho(u_{i+2}+u_i)}{(1+\rho^2)}\right)^2\right]. \end{aligned} \tag{5.18}$$

[10] The abbreviation *i.i.d.* stands for *independent and identically distributed.*

For $\rho = 0$, this becomes:

$$p(\xi_1|\xi_2, u_i) = p(\xi_1|u_i) = \exp\left[-\frac{1}{2\sigma^2}(\xi_1 + u_i)^2\right] = p(u_{i+1}), \quad (5.19)$$

and for $\rho = 1$:

$$p(\xi_1|\xi_2, u_i) = p(\xi_1|\xi_2) = \frac{1}{\sqrt{2}} \exp\left[-\frac{1}{\sigma^2}\left(\xi_1 - \frac{\xi_2}{2}\right)^2\right]. \quad (5.20)$$

With increasing value of ρ, the process becomes more correlated and less stationary, and the conditional density $p(\xi_1|\xi_2, u_i)$ becomes *increasingly independent* of u_i. However, for the stationary process with $\rho < 1$, Eq. (4.13) can not be fulfilled exactly because of the 'restoring force' expressed by ρu_{t-1}, which tends to drive the system back to its long-term mean value, $\overline{u} = 0$.

This behavior is in good agreement with the results on the velocity-dependence of the conditional increment PDFs and the Fokker-Planck equation presented in Sections 4.3 and 5.4.2. At large scales, the turbulence signal becomes more uncorrelated and more stationary, and therefore more similar to white noise. At these large scales, the dependence of the conditional PDF $p(\xi_1|\xi_2, u_i)$ on the velocity u_i is more pronounced, as we would expect from the behavior of the autoregressive process for small values of ρ.

5.4.2 Dependence of conditional PDFs of velocity increments on the velocity

In order to quantify differences of the two distributions in Eq. (4.13), $p(\xi_1|\xi_2, u_i)$ and $p(\xi_1|\xi_2)$, for various different scales r_1 and $r_2 = 2r_1$, we can also apply the Wilcoxon test described in Section 4.5. Figure 5.7 shows the results of the Wilcoxon-test of Eq. (4.13) for three different data sets for different values of u_i as functions of the scale r_1. Values of the test statistics $\langle \Delta Q^* \rangle$ close to one indicate validity of the hypothesis expressed in Eq. (4.13). Due to the nature of statistical tests, the values $\langle \Delta Q^* \rangle$ show some scattering which we attenuate by a moving-average filter with a triangular kernel.

For the free jet and fractal grid, the Wilcoxon test values for the condition $u_i = 0$ are close to one for scales r_1 smaller than approximately half the integral length L (for the free jet, $L \approx 9\lambda$, and for the fractal

grid, $L \approx 8\lambda$). However, for other values of u_i, especially for $u_i = 2\sigma_u$, the range of Wilcoxon test values close to one is reduced to very small values of $r_1 \ll L$. For the cylinder wake, the increase of the test values $\langle \Delta Q^* \rangle$ sets in at even smaller scales (here, however, we have to take into account the relatively large scale separation $L/\lambda \approx 30$). The relatively large values of $\langle \Delta Q^* \rangle$ for very small scales $r_1 < l_{EM}$ might be related the fact that the stochastic process in scale has no Markov properties at scales $r_1 < l_{EM} \approx 0.8\lambda$.

In conclusion, we find only a small range of scales $l_{EM} < r_1 \ll L$, where the Wilcoxon test indicates the validity of Eq. (4.13). In this very small range, the conditional PDFs of the velocity increments are approximately independent of the velocity itself. For larger scales, the velocity dependence of the interscale process can not be neglected. This result is in agreement with the finding presented in Fig. 4.4 in Section 4.3 that the velocity-dependent term d_{10} in the Fokker-Planck equation is quite small at scales $r \ll L$.

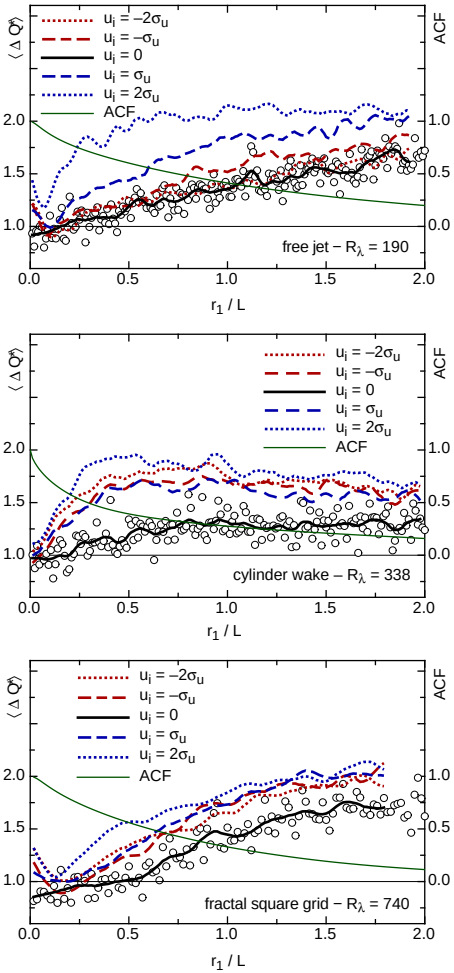

Figure 5.7: Wilcoxon-test of Eq. (4.13) for the free jet and cylinder wake (see Chapter 4), and the fractal grid (see Chapter 2). Circles denote the Wilcoxon-test values $\langle \Delta Q^* \rangle$ for $u_i = 0 \pm \sigma_\xi/8$, and the thick solid line is the smoothed curve of these values, where the smoothing kernel has a triangular shape which includes fife neighboring points to the left and to the right. The dashed and dotted lines are the smoothed curves of the $\langle \Delta Q^* \rangle$ for $u_i = \sigma_u \pm \sigma_u/6$, $u_i = -\sigma_u \pm \sigma_u/6$, $u_i = 2\sigma_u \pm \sigma_u/4$, and $u_i = -2\sigma_u \pm \sigma_u/4$, as denoted in the legends. The decreasing thin solid line is the autocorrelation function ACF $= \langle u(x)u(x+r_1)\rangle / \langle u^2(x)\rangle$.

Bibliography

[1] A. S. Monin and A. M. Yaglom. *Statistical Fluid Mechanics: Mechanics of Turbulence*, volume 1. The MIT Press, 1975.

[2] R. Friedrich and J. Peinke. Description of a turbulent cascade by a Fokker-Planck equation. *Phys. Rev. Lett.*, 78:863–866, 1997.

[3] S. Lück, C. Renner, J. Peinke, and R. Friedrich. The Markov–Einstein cohernce length—a new meaning for the Taylor length in turbulence. *Phys. Lett. A*, 359:335–338, 2006.

[4] C. Renner, J. Peinke, and R. Friedrich. Experimental indications for Markov properties of small-scale turbulence. *J. Fluid Mech.*, 433:383–409, 2001.

[5] C. Renner, J. Peinke, R. Friedrich, O. Chanal, and B. Chabaud. Universality of small scale turbulence. *Phys. Rev. Lett.*, 89:124502, 2002.

[6] M. Tutkun, P. B. V. Johansson, and W. K. George. Three-component vectorial proper orthogonal decompositon of axisymmetric wake behind a disk. *AIAA Journal*, 46:1118, 2008.

[7] F. C. Kaminsky, R. H. Kirchhoff, C. Y. Syu, and J. F. Manwell. A comparison of alternative approaches for the synthetic generation of a wind speed time series. *J. Sol. Energy Eng.*, 113:280–289, 1991.

Erklärung

Ich erkläre hiermit, dass ich diese Arbeit selbstständig verfasst und nur die angegebenen Hilfsmittel benutzt habe.

Oldenburg, den 31. Januar 2011

.....

(Robert Stresing)

In dieser Arbeit enthaltene Publikationen:

R. STRESING, J. PEINKE, R. E. SEOUD, and J. C. VASSILICOS, Defining a new class of turbulence, *Physical Review Letters* **104**, 194501, 2010.

J. Peinke und J. C. Vassilicos hatten bei dieser Arbeit eine betreuende Funktion. J. C. Vassilicos stellte darüber hinaus die Abbildungen 2.1 und 2.5 zur Verfügung. R. E. Seoud führte die Messungen der fraktal erzeugten Turbulenz am Imperial College London durch und stellte die Daten zur Analyse bereit. Die wissenschaftliche Ausarbeitung stammt von R. Stresing.

R. STRESING, D. KLEINHANS, R. FRIEDRICH, and J. PEINKE, Markov properties of homogeneous trubulence, *Physical Review E*, eingereicht 01/2011 (erste Version eingereicht 4/2010).

J. Peinke hatte bei dieser Arbeit eine betreuende Funktion und gab zusammen mit D. Kleinhans und R. Friedrich Anregungen für die Ausarbeitung. Die wissenschaftliche Ausarbeitung stammt von R. Stresing.

R. STRESING and J. PEINKE, Towards a stochastic multi-point description of turbulence, *New Journal of Physics* **12**, 103046, 2010.

J. Peinke hatte bei dieser Arbeit eine betreuende Funktion. Die wissenschaftliche Ausarbeitung stammt von R. Stresing.

R. STRESING, M. TUTKUN, and J. PEINKE, Spatial multi-point correlations in inhomogeneous turbulence, in J. PEINKE, M. OBERLACK, and A. TALAMELLI (eds.), *Progress in Turbulence III – Proceedings of the iTi Conference in Turbulence 2008*, Springer, 2009.

J. Peinke hatte bei dieser Arbeit eine betreuende Funktion und M. Tutkun stellte die von ihm gemessenen Daten zur Verfügung. Die wissenschaftliche Ausarbeitung stammt von R. Stresing.

Weitere Publikationen:

R. STRESING, D. LINDENBERGER, and R. KÜMMEL, Cointegration of output, capital, labor, and energy, *The European Physical Journal B* **66**, 279–287, 2008

Akademischer Lebenslauf

Persönliche Daten:

Name	Robert Stresing
Geburtsdatum	31.01.1979
Geburtsort	Wilhelmshaven
Nationalität	deutsch

Bildung:

08/1985 – 07/1998	Schulbesuch und Abitur in Wilhelmshaven
10/1999 – 06/2005	Studium der Physik an der Universität Würzburg; Vordiplom 10/2001, Diplom 06/2005
08/2002 – 07/2003	Studium der Physik an der University of New Mexico, Albuquerque, USA; M.Sc. in Physics 08/2003
05/2004 – 05/2005	Diplomarbeit bei Prof. Dr. R. Kümmel am Institut für Theoretische Physik der Universität Würzburg zum Thema “Energie und Wirtschaftswachstum”
08/2005 – 08/2010	Doktorarbeit bei Prof. Dr. J. Peinke im Fachbereich Physik der Carl von Ossietzky Universität Oldenburg

Danksagung

Prof. Dr. Joachim Peinke danke ich für die Betreuung, die vielen Ideen, Erklärungen und Gespräche, für seinen Enthusiasmus für unser Forschungsgebiet und für die zahlreichen Gelegenheiten, unsere Arbeit auf Konferenzen präsentieren zu können. Ganz besonders danke ich ihm für seine verständnisvolle Art und seine Vorstellung von der 'akademischen Freiheit' im besten Sinne, durch die die hervorragende Arbeitsatmosphäre in unserer Gruppe nicht zuletzt ermöglicht wird.

Meinen Zweitgutachtern und Prüfern *Prof. Dr. Rudolf Friedrich* und *Prof. Dr. Andreas Engel* danke ich für ihre intensive Beschäftigung mit meiner Arbeit und für die Anregungen, die daraus hervorgegangen sind.

Dr. Stephan Lück, Dr. Christoph Renner, Dr. Murat Tutkun, Dr. Richard Seoud und *Prof. Dr. Christos Vassilicos* danke ich für die hervorragenden experimentellen Daten, welche die Grundlage der vorliegenden Arbeit bilden. Das Kapitel über fraktal erzeugte Turbulenz ging aus einer überaus fruchtbaren Kooperation mit *Christos Vassilicos* und seiner Arbeitsgruppe am Imperial College in London hervor, von dem ich viel über Turbulenz gelernt habe und dem ich für die vielen Einladungen, Gespräche und Anregungen zutiefst dankbar bin.

Dr. David Kleinhans gilt mein ganz besonderer Dank für seine wertvollen Anregungen und Ideen für die in den Kapiteln 3 und 5 präsentierten Arbeiten und für die interessanten Diskussionen über diese und viele andere Themen.

Der DFG danke ich für finanzielle Unterstützung aus dem Projekt PE 478/14-1.

Dr. Michael Hölling, Mathias Hölzer, Pascal Knebel, Agnieszka Parniak und besonders *Gerrit Wolken-Möhlmann* danke ich für die tatkräftige Unterstützung bei experimentellen Arbeiten. *Dr. Andreas Nawroth* danke ich für die Einarbeitung in die Programmierung der stochastischen Analysemethoden.

Dr. Edgar Anahua, Jörg Dapperheld, Arnold Gräbeldinger, Thomas Greve, Dr. Julia Gottschall, Dr. Gerd Gülker, Ali Hadjihosseini, Hendrik Heißelmann, Tim Homeyer, Fatima Keshtova, Michael Langner, Anne Laupichler, Sebastian Marten, Wided Medjroubi, Patrick Milan, Allan Morales, Tanja Mücke, Jarek Puczylowski, Erwin Renken, Philip Rinn, Stanislav Rockel, Anne Schmidt, Jörge Schneemann, Dr. Bernhard Stoevesandt, Stefan Weitemeyer, Dr. Matthias Wächter und den anderen, bereits erwähnten gegenwärtigen und ehemaligen Mitgliedern unserer Arbeitsgruppe danke ich für die vielfältige Hilfe bei kleineren und größeren Problemen von der Programmierung bis zum Windkanal-Umbau, und vor allem für die unvergesslich gute und freundschaftliche Stimmung in unserer Arbeitsgruppe.

Meinen Eltern danke ich dafür, dass sie mir das Studium und damit die Promotion ermöglicht und mich immer darin unterstützt haben.

Meiner Frau *Carmen* gilt mein ganz besonderer Dank für ihr Verständnis für alle Frustrationen des Doktorandendaseins und für ihre unermüdliche ‘moralische’ Unterstützung. Ihr widme ich diese Arbeit.